FACULDADE DE ENGENHARIA DA UNIVERSIDADE DO PORTO

Relative acoustic localization with USBL (Ultra-Short Baseline)

Paula Alexandra Agra Graça

Master in Electrical and Computers Engineering

Supervisor: José Carlos Alves

Co-supervisor: Bruno Ferreira

September 21, 2020

Resumo

Dispositivos robóticos programáveis como *Autonomous Underwater Vehicles* (AUVs) são excelentes meios para exploração subaquática, já que são capazes de executar missões de longa duração com variadas possibilidades de aplicação e objetivos. Neste sentido, o conceito de mula AUV surgiu como mecanismo útil que periodicamente recolhe dados dos AUVs em missão. Para que tal seja possível, é necessário implementar um sistema de localização e posicionamento robusto que permite aos AUVs encontrarem outros veículos de forma a aproximarem-se deles eficientemente.

A presente dissertação foca-se na implementação de mecanismos que levam a um aumento de precisão na localização subaquática usando um sistema USBL (Ultra-Short Baseline), para curtas e longas distância. Primeiro, é descrito o design da arquitetura de um modulo capaz de melhorar a precisão da medida dos tempos de chegada de sinais enviados por uma fonte acústica. De seguida, é conduzido um estudo sobre possíveis métodos de avaliação do desempenho de uma configuração de sensores, já que consiste num aspecto crucial na precisão de estimação. Por último, o método de seleção adaptativa de configurações é apresentado, o qual serve como ferramenta que seleciona um conjunto de hidrophones, a partir de um grupo discreto em posições fixas, que leva a uma maior precisão na localização. Este método pretende retificar problemas que surgem em sistemas USBL clássicos.

Após a implementação, todos os mecanismos desenvolvidos foram sujeitos a testes detalhados em simulação que validam o seu funcionamento e demonstram resultados satisfatórios em condições controladas. Adicionalmente, foram realizados testes no tanque do DEEC e em mar aberto para avaliar as melhorias alcançadas nas medidas dos tempos de chegada.

Abstract

Robotic programmable devices such as Autonomous Underwater Vehicles (AUVs) are great means for underwater exploration, as they are capable of executing long term missions with many possible applications and goals. In this regard, the concept of mule AUVs arises as a valuable mechanism to periodically collect data from survey AUVs during the missions. In order to achieve this, a robust localization system needs to be implemented allowing the mule AUV to find the other vehicle and draw near it efficiently.

The present dissertation focuses on the implementation of mechanisms that lead to an increase in underwater localization precision using an USBL (Ultra-Short Baseline) system, for both short and long range. Firstly, it is described the architecture design of a module that is capable of improving the precision of the time of arrival measurement of signals sent by an acoustic transmitter. Then, a study is conducted on possible methods for evaluating a sensor configuration performance, as it consists on a crucial aspect in estimation precision. Lastly, the adaptive configuration selection method is presented, which serves as a tool that selects a set of hydrophones, from a discrete group in fixed positions, that leads to the highest localization precision. This method intends to rectify issues that arise from classic USBL systems.

After implementation, all developed mechanism were subjected to comprehensive simulated tests that validate its function and demonstrate successful results with controlled conditions. Additionally, tests were performed in DEEC's tank and in open sea to evaluate the achieved improvement on the time of arrival measurements.

Agradecimentos

Aos meus orientadores: professor José Carlos Alves, pelo incansável apoio, inspiração e motivação desde o primeiro ano de faculdade, e Bruno Miguel Ferreira, pela disponibilidade, interesse e constante incentivo.
À FEUP, por testar o meu limite em todos os sentidos, e ao projeto GROW desenvolvido pelo CRAS (INESC TEC), por me abrir portas a desafios interessantes num tema que me relembrou a razão pela qual quis seguir engenharia.
Aos amigos da faculdade e do IEEE UP SB, por me guiarem numa realidade que me vai sendo cada vez menos desconhecida, por me inspirarem a establecer objetivos ambiciosos para mim própria, pelas longas noites, pela melhor experiência de sempre em Munique.
Aos amigos de longa data, por me relembrarem das minhas raízes e de quem sou, pelas conversas intermináveis, pelos abracinhos e pelo apoio incondicional.
Ao meu namorado, por todas as experiências, pela paciência interminável, por me levares sempre contigo e simplesmente acreditares.
Aos meus pais e irmã, pelos miminhos e por tornarem tudo isto possível.

Paula

"A curiosidade leva por um lado a escutar às portas
e por outro a descobrir a América"

Eça de Queirós

Contents

List of Figures

List of Tables

Abbreviations

ADC	Analog to Digital Converter
AUV	Autonomous Underwater Vehicle
BPSK	Binary Phase Shift Keying
CC	Cross-Correlation
CORDIC	COordinate Rotation DIgital Computer
CRLB	Crámer-Rao Lower Bound
DEEC	Departamento de Engenharia Electrotécnica e de Computadores
FIM	Fisher Information Matrix
FIR	Finite Impulse Response
FPGA	Field-Programmable Gate Array
FSK	Frequency-Shift Keying
GCC	Generalized Cross-Correlation
HDL	Hardware Description Language
LBL	Long Baseline
LOS	Line-of-sight
LUT	Lookup Table
MF	Medium Frequency
ML	Maximum Likelihood
PSK	Phase Shift Keying
PSO	Particle Swarm Optimization
RMS	Root Mean Square
ROM	Read-Only Memory
RSSI	Received Signal Strength Indicator
SBL	Short Baseline
SNR	Signal-Noise Ratio
TDE	Time Delay Estimation
TDoA	Time Difference of Arrival
ToA	Time of Arrival
ToF	Time of Flight
USBL	Ultra-Short Baseline

Chapter 1

Introduction

This chapter intends to specify the context of the present dissertation, describing the considered scenario, technologies and conditions in which the proposed solution is useful. Based on this, the two main goals of the present research work are established. Lastly, it is explained how the document is structured, including a concise summary of each chapter's content.

1.1 Context and Motivation

Today, the deep blue ocean still represents a relevant topic of research in the scientific community as it constantly rises new unexplained mysteries. Up to now, only 15% of the entire ocean floor is mapped based on collected data [1]. As such, it seems essential to create efficient research tools to improve the discovery of information.

Robotic autonomous underwater vehicles (AUVs) are great means for diverse applications in underwater exploration using variable resource requirements and duration, such as monitoring structures installed in shallow waters or exploring the deep ocean floor for scientific purposes. Particularly in long-term missions, the AUV usually navigates underwater, resorting to docking systems to allow extended navigation periods, until the end of the mission when it returns to the base station. Thus far, the data that is being collected is typically not accessible by any processing system.

A method that is used to resolve this limitation is employing additional mule AUVs, whose goal is to travel near the survey AUV, collect its data during the mission's term and return in a relatively short time period. This allows the data to be periodically processed during the mission, which facilitates the definition of future courses for the mission, such as shortening its duration or sending additional commands. In the mentioned localization system, high precision is key as it allows the AUVs to reach very short distances between them when they approach each other. This typically influences the achievable debit of data transfer in common communication solutions, which is a key aspect in data muling.

The described process can only be achieved if the mule AUV is able to locate the other vehicle and draw near it. For such application, USBL (Ultra-Short Baseline) systems prove to

have several advantages comparatively to other localization methods, such as optical, radio and inertial based techniques. The main advantages are the achievable range, limited error and lower sensibility to environment conditions, such as salinity or turbidity. For that reason, in this scenario, a USBL system is used to receive the transmitted signals and calculate the angle of arrival of the acoustic signal, thus the direction that the mule AUV should navigate. Additionally, using a synchronization mechanism, the mule is also able to determine the distance to the acoustic source and thus the vehicles' relative positions.

In such scenario, the USBL system needs to meet specific requirements to assure a reliable localization. Since the acoustic source can be located anywhere, it is essential that the estimation is accurate for both short and long range distances. Additionally, the system needs to have line of sight in any direction, which is compromised from the start by deploying the sensors on an AUV. Typically, the available USBL commercial solutions do not tackle these issues simultaneously, so the development of such system constitutes a technological challenge.

Therefore, this dissertation intends to develop a method that improves relative localization of AUVs using reconfigurable USBL systems. All the contemplated tools and complementary mechanisms are carefully explained throughout the document.

This research work falls under the scope of activities developed by the Center of Robotics and Autonomous Systems of INESC TEC. It is integrated in the GROW project which focuses on exploring the use of AUVs as data mules for long duration missions.

1.2 Objectives

The goal of the present work is to study and propose an adaptive configuration selection method, which assumes the integration of several hydrophones in a USBL system to allow selecting the set of sensors that minimizes the estimation error. This aims to achieve high estimate accuracy for both short and long range distances and continuously provide a set of hydrophones that have line of sight with the target, which can be located anywhere. In order to attain this, a comparative study is developed on tools that allow to compare the performance of sensors configurations in order to select the most reliable option. Then, the proposed system is presented in detail and validated with comprehensive simulations.

Building upon previous developments on the USBL system, it is also intended to achieve a more rigorous calculation of the TDoA to enable a more precise localization. By associating this improved calculation with the correlation measurement already implemented, it is expected to obtain a more precise ToA measurement.

1.3 Document Structure

The present document is partitioned into six chapters, which are summarized in this section.

Chapter 2 offers an overview on background concepts about underwater acoustics, localization estimation and positioning systems, followed by USBL available commercial

solutions and developed technology for a similar purpose. Lastly, it focuses on optimization mechanisms that are typically employed for evaluating sensor configurations.

After reviewing the literature, chapter 3 intends to clarify the problem that is being resolved in this thesis. The work assumptions are laid out followed by the statement of the research hypothesis and the research questions that are intended to be further explored. The chapter ends with the clarification of the used validation methods for the work.

Chapter 4 explains the implemented digital signal processing module for the phase difference calculation, describing its components and design decisions. At the end, the influence of the Doppler effect is studied.

Chapter 5 presents three different approaches are presented for systematic comparison between the performance of a sensor configuration. These are supported with simulation experiments which allow to draw conclusions on the preferred approach.

Chapter 6 details the developed dynamically reconfigurable configuration method. The theoretical specifics and thought process are laid out and the mechanism is then validated through simulations.

Lastly, chapter 7 gives the final remarks about the developed work, enumerates the contributions and mentions research work which could be further developed in the future.

Chapter 2

State of the Art

This chapter presents the fundamental concepts of underwater acoustics engineering for localization and positioning of aquatic autonomous vehicles.

2.1 Underwater Acoustic Channel

Although satellite based navigation systems are the most commonly used for positioning and localization at the earth surface, the used radio signals are highly absorbed by the water and thus inappropriate for underwater localization and communications. Therefore, the state of the art solutions for long range localization and communications in the underwater environment rely on the propagation of acoustic signals.

The natural limitations of acoustic channels combined with the properties of an underwater environment, result in challenges and limitations in developing communication and localization systems [2]:

- Long propagation delays make it unmanageable for underwater acoustic networks to employ some common data networks' mechanisms, such as acknowledgment-based protocols;
- Variable speed of the acoustic signals due to variations in temperature and density;
- Limited bandwidth, as the attenuation of acoustic waves increases with frequency;
- The path of acoustic signals is not a straight line since the sound waves are bent due to sound speed variation along the water column and reflected or blocked in many different surfaces and objects, which may lead to the incorrect detection of the line-of-sight (LOS) signal;
- Attenuation and asymmetric signal-to-noise ratio, which arises from SNR depending on depth and frequency with complex behaviors that depend on the characteristics of the environment;

Underwater localization systems based on acoustic signals are the only effective way to work in distance ranges up to a few kilometers, as opposed to optical or radio-frequency based systems.

However, these always unreliable characteristics lead to a significant degree of uncertainty as, in practice it is impossible to know the exact speed and path of a sound wave along the path it actually travels.

This section presents hereinafter a more detailed overview on various concepts that affect the underwater communication channels, such as the sound speed, multipath phenomena, the Doppler effect, signal attenuation and signal-to-noise ratio.

2.1.1 Speed of Sound

The oceanic environment has a complex sound propagation model, as it comprises many variants.

Acoustic signals' propagation speed is mainly related to two factors: compressibility and density. The water density can be characterized by the temperature, salinity and pressure,which is associated with depth [3]. Figure 2.1 exhibits a generic sound speed profile in relation to depth. The water surface is commonly a mixed layer that results in an approximately constant sound speed. After this layer, it suffers a significant decrease, usually reaching the lower tangible speed, which results from the variation of temperature that characterizes the thermocline layer. From that point forward, pressure is the greatest influencer on speed of sound, so it increases relatively proportionally to depth.

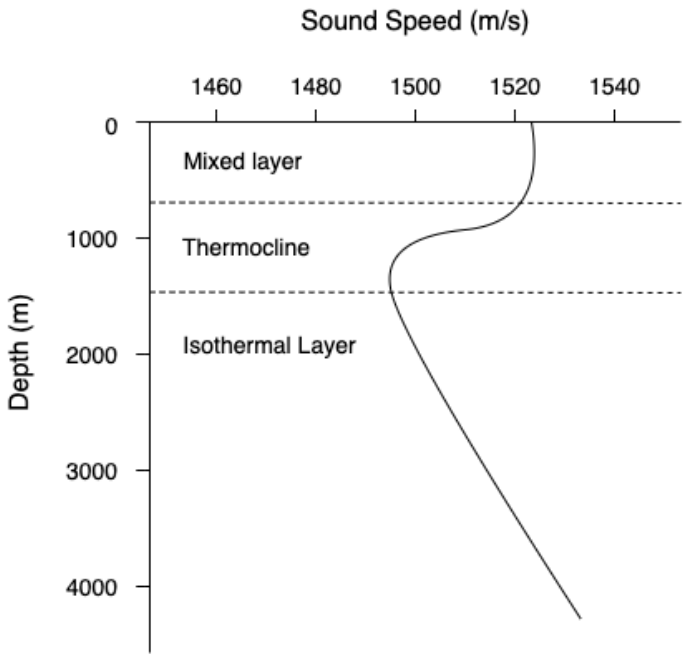

Figure 2.1: Generic sound speed profile

The empirical equation (2.1) [3] is a simplified translation of the behavior of the sound speed c in meters per second, with relation to the temperature T in ^{o}C, the salinity S in parts per thousand

and the depth z in meters.

$$c = 1449.2 + 4.6T - 0.055T^2 + 0.00029T^3 + (1.34 - 0.01T)(S - 35) + 0.016z \quad (2.1)$$

The varying sound speed throughout the water column causes the signals not to propagate in a straight line from a transmitter to a receiver. Therefore, the ToA calculation would not be precise in positioning system such, as USBL.

2.1.2 Multipath

Multipath occurs when signals suffer distortion that originate multiple propagation paths, leading to a change in their original characteristics. This phenomenon is originated by diverse factors that cause distortion in the underwater channels, typically affecting the water composition, such as water temperature and depth. The signal distortions caused by multipath include signal fading, which is usually modeled by Rayleigh fading channel theory [4], varying operation frequency, time-variant propagation delays, among others.

The multipath behavior can be distinguished depending on depth, in shallow water paths and deep water paths since they demonstrate distinct propagation effects:

Shallow water paths In shallow water, the acoustic signals can be reflected or refracted on the surface, where attenuation is generally weaker then at the bottom of the ocean. There it suffers a higher attenuation depending on the soil material, frequency and incidence angle. Figure 2.2 represent a typical multipath caused by reflection on the sea surface and bottom.

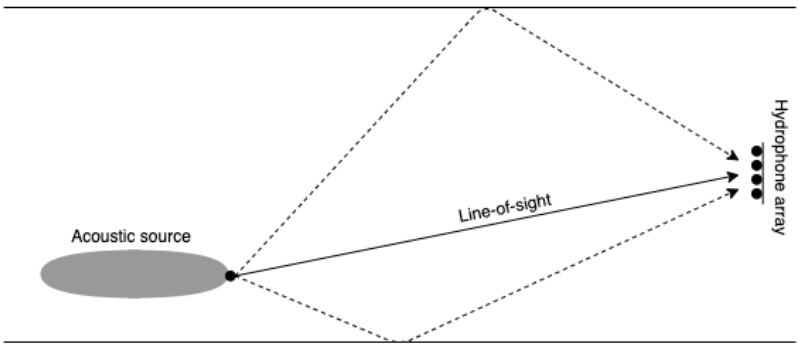

Figure 2.2: Illustrative example of shallow water multipath

Deep water paths In deep water, there are essentially six types of propagation paths, detailed bellow, whose channel model equations can be consulted in [4]. These rely on the notion that signals are bent towards the characteristics that lead to a slower propagation speed, such as a temperature and depth decrease.

- *Surface reflection*: the signal is reflected on the sea surface, where the attenuation depends on its acoustic roughness.

- *Surface duct*: the signal gets confined in a surface layer, where the sound velocity increases with depth, due to varied thermal conditions in deeper layers, which causes it to bend the wave path to the surface and bounce back when reaching the subsequent layer.
- *Bottom bounce*: the signal is reflected on the bottom of the ocean, suffering attenuation dependent on the soil material.
- *Convergence zone*: it depends on the sound speed profile and water depth that characterizes the channel. When the temperature decreases the signal has a tendency to bent downwards, however when an increase in pressure is reached the signal tends to bent upwards again, originating convergence locations.
- *Deep sound channel*: it is originated in levels that are surrounded by layers with characteristics highly dependent on depth. So, the signal is constantly bent according to the depth that leads to a minimum speed.
- *Reliable acoustic path*: this path occurs when the transmitter is positioned in very deep water and the receiver is near the surface. Although the signal is bent downwards due to decreased temperature, when it reaches a certain depth it is bent upwards making the communication channel reliable.

The multipath phenomena is a very common factor that affects underwater communication mechanisms such as the USBL systems. For such case, the ray bending that occurs between the transmitter and the receiver can cause the signal to assume different paths and affect the resulting estimations. For instance, if the signal deviates from the direct path, then the angle of arrival would not be accurate and the ToA increases leading to an increased error on the range estimation.

2.1.3 Doppler Effect

In a communication and localization system between two entities moving with non-zero relative velocity, if a transmitter sends a signal with a certain operation frequency to the receiver, then the perceived frequency by the receiver will suffer a shift from the original signal. This frequency difference is expressed as a Doppler shift and explained by the Doppler Effect.

The magnitude of the generated frequency shift can be expressed as a ratio (2.2), where the transmitter-receiver velocity is compared to c, the speed of sound [5].

$$a = \frac{v}{c} \tag{2.2}$$

Autonomous Underwater Vehicles (AUVs) usually move with velocities in the order of few meters per second. Therefore, the a factor mentioned above has a significant value and needs to be considered when implementing synchronization systems, as well as developing estimation algorithms.

In certain localization and communication systems, it is critical to correct the Doppler effect because data can be compromised (e.g. FSK modulated signals, in which information is codified into frequency changes). A simple Doppler compensation process was proposed in [6], with the intent of integrating it in a system that detects phase-modulated binary sequences using cross-correlation.

This phenomenon can also be explored to determine the relative velocity between two devices, by measuring the frequency deviation with respect to the frequency expected to be received.

The Doppler effect can influence the USBL system's performance since the computation of TDoAs depend on the perceived phase difference between the arriving signals, which are directly related to the operation frequency. Therefore, a frequency shift would make the positioning system have a distorted perception of the phase differences and thus the signal's angle of arrival.

2.1.4 Attenuation and Signal-to-Noise Ratio

When considering underwater communication systems, it is essential to quantify the attenuation of the channel, i.e. the part of the signal's energy that is absorbed by the surroundings. In underwater channels, this absorbance is frequency variable and also depends on physical characteristics of the water, as salinity and temperature.

The underwater acoustic channel has a particular model that describes its attenuation path loss $A(d,f)$, given in logarithmic scale by equation (2.3) [7].

$$10\ log(A(d,f)) = 10\ k\ log(d) + d \times 10\ log(a(f)) \tag{2.3}$$

From the equation, d is the distance from the transmitter to the receiver in kilometers (Km), f is the operating frequency in kilohertz (KHz), $10klog(d)$ represents the spreading loss that describes how the sound level (in decibel, dB) decreases as the sound wave spreads, $d \times 10\ log(a(f))$ is the absorption loss that a signal suffers during its propagation path, k is the spreading factor that is related with the considered configuration (e.g. cylindrical, spherical, etc.), $a(f)$ is the absorption coefficient that can be obtained through the equation in [7].

Noise is another factor that is considered when analyzing a real underwater acoustic channel, as it defines the signal-to-noise ratio (SNR) that characterizes the channel. The SNR depends on the attenuation level, which increases with frequency, and the noise, which decays with frequency. Consequently, the SNR varies over the signal bandwidth and it is asymmetric. The equation (2.4) [5] expresses this relationship, where $S_d(f)$ represents the power spectral density of the transmitted signal.

$$SNR(d,f) = \frac{S_d(f)}{(A(d,f))\ N(f)} \tag{2.4}$$

Signals that are heavily attenuated can become an issue when dealing with acoustic positioning systems, such as USBL systems. If the transmitted signals suffer high attenuation then it can be unfeasible to rigorously detect the signal in the receiver, therefore compute the

range or angle of arrival of the transmitter. Additionally, in case of having a noisy environment it can be difficult to identify the intended acoustic signal, since it can be blended with the noise and not be distinguishable.

2.2 Underwater Localization Estimation

This section focuses on two categories of the underwater localization estimation, namely methods based on range estimation and algorithms of position estimation based on reference nodes.

2.2.1 Range Estimation

Underwater localization takes into consideration the distance between the target object to track and the reference point. As consequence, it is relevant to apply methods that effectively determine this range.

There are two main types of techniques that are used to achieve such objective: the Received Signal Strength Indicator (RSSI) and the Time Delay Estimation (TDE).

2.2.1.1 Received Signal Strength Indicator

The Received Signal Strength Indicator (RSSI) method is based on the strength of the signal that reaches the target. It determines the distance between the target and the reference node by analyzing the received signal strength and comparing it with an underwater attenuation model that is range dependent [3].

Since the underwater acoustic channel suffers from multipath, time variance and high overall path loss, the RSSI technique is typically not adequate for long range underwater applications. However, in short range communications such effects can be sufficiently attenuated for this technique to be used.

2.2.1.2 Time Delay Estimation

Time Delay Estimation (TDE) mechanisms imply a pair of nodes, the transmitter and the receiver, to measure the range between them. This distance is based on the time that it takes for a signal to travel from the reference point to the target. The accuracy of these techniques depends mainly on the environment conditions, which include the water properties and the surrounding reflection surfaces that cause multipath. Therefore, the mechanisms are susceptible of variable errors according to the location and characteristics of its employment.

There are three main categories that divide TDE methods, which are Time of Arrival (ToA), Time of Flight (ToF) and Time Difference of Arrival (TDoA).

Time of Arrival Time of Arrival (ToA) is interpreted as the time delay between the transmission of a signal in the reference node until its reception on the target node. Although this is the

conceptually simplest method to employ, it requires synchronization between the nodes since the target entity needs to know the instant when the signal was sent to be able to calculate the difference.

Considering a generic transmitted signal *s(t)*, the received signal can be expressed as (2.5), where τ represents the time of arrival and *n(t)* is white noise with zero mean [8].

$$r(t) = s(t-\tau) + n(t) \tag{2.5}$$

Time of Flight Time of Flight (ToF) measures essentially the round-trip travel time between two nodes. The transmitter node sends a query signal to the receiver node, which has an integrated transponder that responds transmitting a signal back within a know time delay. The ToF is then estimated as the time interval from the moment the first signal is transmitted until the moment the second signal is received by the same node.

This method may be used without additional synchronization systems as it assumes that the response signal is sent after the received one and the intrinsic transmitting delays are known.

Time Difference of Arrival The Time Difference of Arrival (TDoA) is a technique that compares the time of arrival of a signal to different hydrophones in order to estimate the angle of arrival of the acoustic signal. The array of reception hydrophones have known relative positions among them so that is is possible to compare the different times of arrival or phase differences. This method can be employed using a uni-directional signal or a round trip communication.

There are several algorithms and mathematical models that can be employed to execute the TDoA method, such as Cross-Correlation and Maximum Likelihood.

- **Cross-Correlation**

  The Cross-Correlation (CC) method is used to represent the strength relationship between two signals.

  Considering two distanced hydrophones in the same environment and an acoustic signal *s(t)*, $x_1(t)$ and $x_2(t)$ are the signals received by each of the two hydrophones. Equations (2.6) and (2.7)[9] express the mentioned signals in relation to $w_1(t)$ and $w_2(t)$ that are Gaussian noise coefficients uncorrelated with the source, the delay τ and an attenuation function α.

$$x_1(t) = s(t) + w_1(t) \tag{2.6}$$

$$x_2(t) = \alpha\, s(t-\tau) + w_2(t) \tag{2.7}$$

  In order to determine the time delay, τ, between signals, the cross-correlation function can be calculated as (2.8). The estimate of the time delay between two signals, τ, is given by $argmax_{\,t\in R^+} Rx_1x_2(\tau)$, which represents the maximum correlation value and it is the main outcome of Time Delay Estimation.

$$R_{x_1x_2}(\tau) = E[x_1(t)\, x_2(t-\tau)] \tag{2.8}$$

However, since the observation time is finite then function $R_{x_1x_2}$ can only be estimated, originating equation (2.9) where T expresses the observation interval.

$$\widehat{R}_{x_1x_2}(\tau) = \frac{1}{T-\tau} \int_{\tau}^{T} x_1(t)x_2(t-\tau)dt \tag{2.9}$$

There are two main variations of CC [10], which are the slow cross-correlation in the time domain, as before mentioned, and the fast cross-correlation in the frequency domain, which is based on the Fast Fourier Transform as it locates the peak by analyzing frequency similarities between the signals.

- **Generalized Cross-Correlation**

  After presenting the cross-correlation method, it is easier to understand the Generalized Cross-Correlation (GCC) method, which is extensively explained in [10]. Recalling the equations that define the CC, the GCC is achieved by prefiltering the x_1 and x_2 prior to the integration in (2.9), using filters H_1 and H_2. Then the obtained filtered signals y_1 and y_2 are multiplied and integrated in a period of time T until detecting the function peak.

  Then the GCC between $x_1(t)$ and $x_2(t)$ is given by (2.10), where the $G_{x_1x_2}(f)$ represents the cross power spectrum between the filter inputs.

$$R_{y_1y_2}(\tau) = \int_{-\infty}^{\infty} \psi(f) G_{x_1x_2}(f)\, e^{i2\pi f\tau} df \tag{2.10}$$

$$\psi(f) = H_1(f)H_2^*(f) \tag{2.11}$$

  The function $\psi(f)$ (2.11), with $*$ denoting the complex conjugate, represents the prefilter and it is essentially the distinctive parameter that originate different methods of cross-correlation, since it should depend on different environments and properties, as SNR. The CC technique uses a prefilter $\psi(f)$ equal to 1, being the simplest method of its kind.

- **Maximum Likelihood**

  The Maximum Likelihood (ML) method is a variation of Cross-Correlation which uses the prefilter $\psi(f)$ represented mathematically by (2.12), where $\gamma_{12}(f)$ is a function of spectrum of cross-correlation $G_{x1x2}(f)$ and spectrum of auto-correlations $G_{x1x1}(f)$, $G_{x2x2}(f)$ as expressed in (2.13) [10].

$$\psi(f) = \frac{|\gamma_{12}(f)|^2}{|G_{x1x2}(f)|[1-|\gamma_{12}(f)|^2]} \tag{2.12}$$

$$|\gamma_{12}(f)|^2 = \frac{|G_{x1x2}(f)|^2}{G_{x1x11}(f).G_{x1x11}(f)]} \tag{2.13}$$

There is also a version of ML that uses the power spectral densities of the signals, which can be helpful for calculations in various applications.

2.2.2 Position Estimation with Reference Nodes

In networks with multiple nodes it is typical to use localization estimation to establish relative positions between elements. This is usually achieved by establishing reference nodes with known positions so that it is possible to determine relative positions based on them.

Two of the most commonly used methods for underwater acoustic positioning are Triangulation, which is based on the angles between nodes and the object to be located, and Lateration, which is based on the range between the element to be located and each node [11]. These methods present two common restrictions: both need of a minimum of three visible nodes for 2D localization or four beacons for 3D localization and both fail to determine the unknown position if the nodes and the position to be estimated are all placed in the same circumference.

An extensive comparison of different localization schemes for underwater sensors networks can be consulted in [12].

2.2.2.1 Triangulation

Triangulation is a method widely used in mobile robot localization so various algorithms have been proposed. In [13], triangulation methods are divided into four categories:

- Geometric Triangulation: comprises methods based on geometric relations and trigonometry;
- Geometric Circle Interaction: the algorithms calculate the radius and center of two circles that pass through the nodes and the object to be localized, so that the intersection between them gives the unknown localization;
- Iterative methods: includes algorithms that iteratively estimate the position by linearization of trigonometric relations;
- Multiple Beacons Triangulation: the methods use more than three angles to localize an object, which is usually used in scenarios with corrupted angle measurements.

Since this method was not adopted in the present dissertation, only a brief overview on the existing algorithms was made.

2.2.2.2 Lateration

The most typically employed lateration technique is the multilateration, which is used in this dissertation. As mentioned before, it relies on the range between the object to be localized and multiple reference nodes. In this method, the employment of *n+1* nodes allows to determine *n* coordinates [14]. For instance, determining the position (x,y,z) of an object requires to resolve a system of equations using (2.14), where (x_i,y_i,z_i) are the coordinates of the node and d_i is the distance between the node and the object.

$$(x-x_i)^2+(y-y_i)^2+(z-z_i)^2=d_i^2 \tag{2.14}$$

Figure 2.3 illustrates a specific case of trilateration, which implies the use of three reference nodes 1, 2 and 3. The object *O* corresponds to the position to be localized that is determined by calculating the intersection between the three circumferences, generated by knowing the relative positions and ranges, d_1, d_2 and d_3, between all elements.

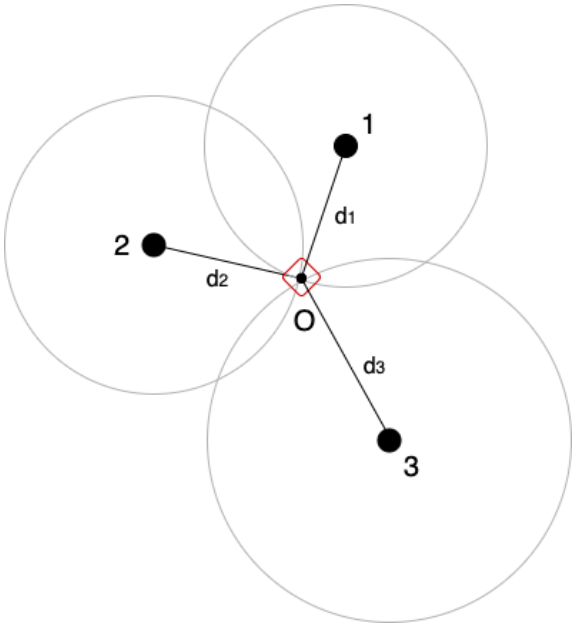

Figure 2.3: Localization using trilateration

Distributed mechanisms, such as multilateration, are usually divided in three phases of positioning [12]:

- Distance estimation between the reference nodes and the target object, usually using TDoA or ToF mechanisms;
- Position estimation, obtained by solving a system of linear equations through mathematical techniques or sensor fusion using an estimator, since the solutions are usually approximated due to noise or non-linearities;

- Final refinement of the measurement in order to improve accuracy.

As an alternative to solve localization issues using circumferences, multilateration can also take advantage of a hyperbola-based localization method. Considering a target at (x,y) and three reference beacon with coordinates (x_i, y_i), (x_j, y_j) and (x_k, y_k), we have that the difference between times of arrival t_i and t_j to nodes i and j, respectively, can be related to the distance between nodes, as expressed in (2.15) [14]. d_i and d_j are the distance from node i and j, respectively, to the target object.

$$d_i - d_j = c * (t_i - t_j) = \sqrt{(x-xi)^2 + y - yi)^2} - \sqrt{(x-xk)^2 + y - yk)^2} \tag{2.15}$$

2.3 Underwater Acoustic Positioning Systems

Positioning systems are used to track the underwater position of a vehicle or other object, in relation to reference structures of transponders called *baseline stations*. These systems are classified based on the distance between the baseline stations. The configurations that will be explained are Long Baseline (LBL), Short Baseline (SBL), Ultra-Short Baseline (USBL) and the inverted versions of all above.

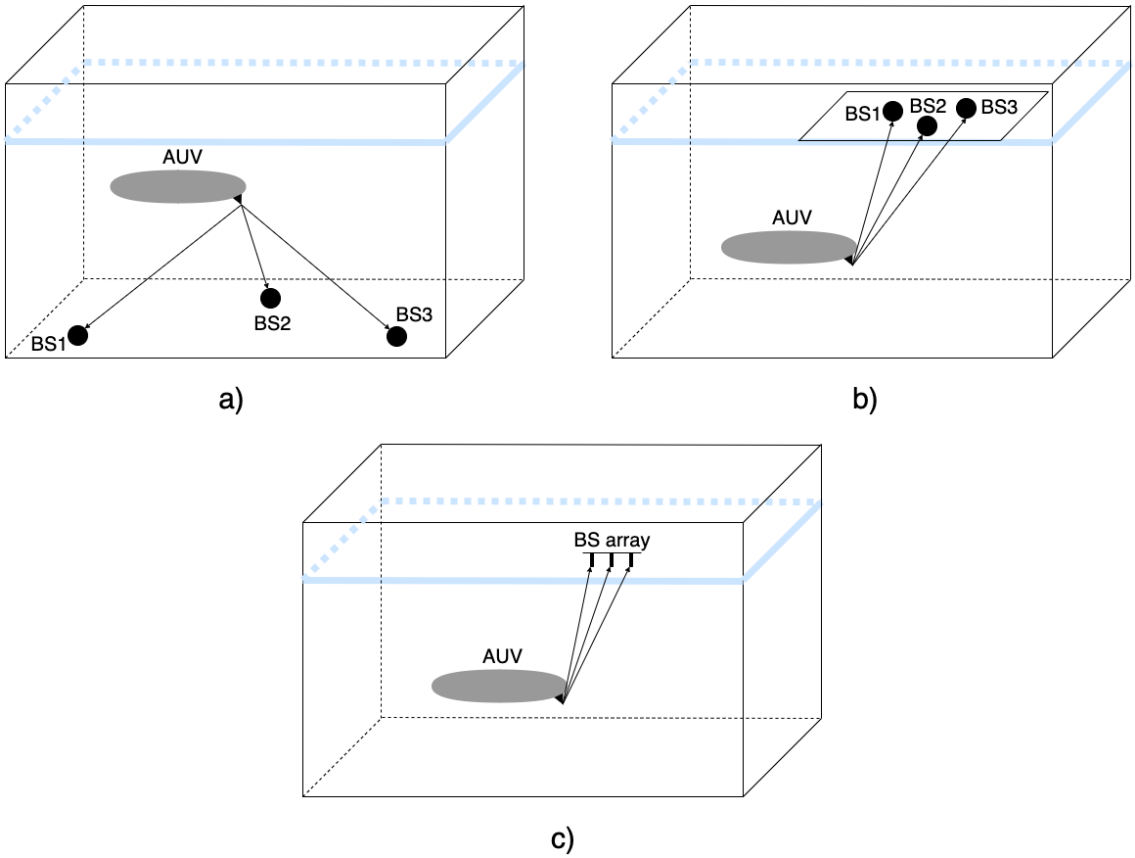

Figure 2.4: Generic configuration of: a) LBL; b) SBL; c) USBL

2.3.1 Long Baseline (LBL) and Short Baseline (SBL)

Long Baseline (LBL) and Short Baseline (SBL) systems are characterized by different ranges and transponder deployment, however they share the same operating procedure.

Long Baseline systems use a positioning method with large distances between baseline stations, with a range typically from $50m$ to more than $2000m$ and usually similar to the distance between the receiver and the transponders [10]. A typical LBL configuration is represented in illustration a) of 2.4. It uses at least three transponder stations deployed usually on the sea floor.

Short Baseline systems are characterized by having distances around $20m$ to $50m$ between baseline stations [2] and uses transponders usually placed in a moving platform, assuring fixed relative position between them. A typical SBL configuration is represented in illustration b) of 2.4.

For both LBL and SBL, a complete localization procedure starts with the vehicle sending an acoustic signal which is received by the transponders. Thereafter the transponders transmit a response and, by analyzing the Time of Flight of the communication,it is possible to determine the distance between the vehicle and each transponder. Then the relative position of the vehicle is determined through trilateration. Considering t_i the propagation time of the signal from the vehicle to the ith transponder, c_s the speed of sound and $(x_{b_i}, y_{b_i}, z_{b_i})$ as the coordinate position of the transponder, then equation (2.16) [15] expresses the position of the vehicle. Additionally, if the transponders have known geographic positions, it is possible to infer the vehicle's absolute geographic position.

$$\sqrt{(x_{b_i}-x)^2+(y_{b_i}-y)^2+(z_{b_i}-z)^2} = c_s * t_i \tag{2.16}$$

The accuracy of these methods depend on several factors, such as the range of communication and transponders configuration, and it typically fluctuates between tens of centimeters and a few meters.

2.3.2 Ultra-Short Baseline (USBL)

Ultra-short Baseline systems are composed essentially by one baseline station, with an array consisting of several traducers distanced typically less than the wavelength [16], and a transponder integrated on the vehicle. It is usually represented as illustration c) of 2.4.

Similarly to the previously mentioned procedures, the USBL positioning method relies on the Time of Flight of the exchanged signals. However, the traducers are too spatially close from each other to execute an accurate trilateration. Instead, it is measured the phase difference or time-delay difference of the received signal between every traducer, in order to estimate the azimuth and distance to the acoustic source.

Assuming a three dimensional scenario for the positioning system, as represented in figure 2.5, the object's coordinates are given by equations (2.18), (2.19) and (2.20) [17]. The λ corresponds

to the wavelength of the of the transmitted signal which depends on its operation frequency, f, and it is affected by the speed of sound c, as represented equation (2.17). The d represents the distance between hydrophones, ψ_{12} and ψ_{22} are the phase difference between H2 and the other two hydrophones, H is the height of the target object, X is the distance of the target along the x-axis direction, Y is the distance of the target along the y-axis direction and l is the slant distance of the target to the hydrophone.

$$\lambda = \frac{c}{f} \tag{2.17}$$

$$l^2 = X^2 + Y^2 + H^2 \tag{2.18}$$

$$\psi_{12} = \frac{2\pi}{\lambda}[\sqrt{l^2} - \sqrt{(d-X)^2 + d^2 + H^2}] \tag{2.19}$$

$$\psi_{22} = \frac{2\pi}{\lambda}[\sqrt{l^2} - \sqrt{X^2 + (d-Y)^2 + H^2}] \tag{2.20}$$

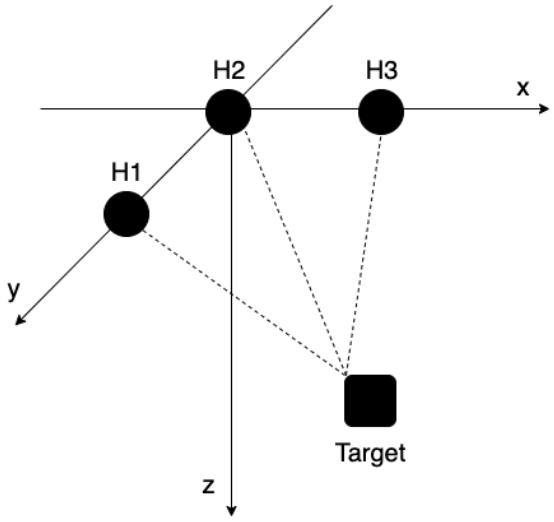

Figure 2.5: USBL system configuration

This is a broadly used technique due to its convenient set up, which allows to have predefined measurements in the order of tens of centimeters and does not require the deployment of support infrastructures in the intended navigation area of the target AUV. However, since the USBL is based on bearing determination it needs high accuracy in order to achieve efficient localization estimations..

2.4 Commercial Solutions

There are several commercial solutions for underwater positioning using the Ultra-Short Baseline method. In this section, some of the available devices in the market will be presented, indicating their main properties and capabilities. Table 2.1 summarizes the systems with most relevance to the present work in terms of used bandwidth, maximum range and precision. The

Medium Frequency (MF) bandwidth is attributed to devices whose manufacturer did not specified the actual frequency range. The specified precision depends on the available information, which varies between slant range precision (SR) and range detection (RD).

Evologics produces the S2C R USBL series of acoustic modems [18], with Sweep Spread Carrier (S2C) technology [19] which uses a broad frequency range to propagate over large distances with reduced noise. The devices have a fixed 0.01m slant range precision and a 0.1 degree bearing resolution. These are essentially divided into two groups:

- High speed mid-range devices: contains the 18/34 transceivers family [20], which presents various options for the USBL antenna beam pattern and it is designed for transmission in horizontal channels.

- Depth rated long-range devices: includes the 12/24 transceiver [21], which have a directional (70 degrees) USBL antenna and it is designed for transmission in vertical channels.

Sonardyne markets the Ranger 2 systems. The Micro-Ranger 2 [22] is appropriate for shallow waters, achieving accuracy of 0.2% with a $3Hz$ position update rate. The Mini-Ranger 2 [23] is intended for nearshore missions and it is used for simultaneous tracking of various mobile targets, whose position update rate is $3Hz$ as well.

Applied Acoustics offers the Easytrak USBL Systems [24], which includes the processing software for estimating the position. The Alpha Portable 2655 consists in a very compact structure that includes an array transducer and is capable of reaching a 10cm slant range resolution and a 2 degree RMS.

Kongsberg produces the HiPAP family of transducers [25], which can use the Cymbal acoustic protocol (PSK) or the frequency shift (FSK) modulation technique. Particularly the HiPAP 352 is the model with higher number of active transducers and is able to reaches 0.02m of range precision.

Company	**System**	**Bandwidth (kHz)**	**Connection (kbps)**	**Max Range (m)**	**Precision**
Evologics	S2C R 18/34D USBL	18-34	up to 13.9	3500	0.01m (RD)
	S2C R 12/24 USBL	12-24	up to 9.2	6000	0.01m (RD)
Sonardyne	Micro-Ranger 2	MF	0.2-9	995	5% (SR)
	Mini-Ranger 2	MF	0.2-9	995	1.3% (SR)
Applied Acoustics	Easytrak Alpha Portable 2655	MF	n.d.	500	3.5% (SR)
Kongsberg	HiPAP 352	21-31	n.d.	5000	0.02m (RD)

Table 2.1: Overview of commercial solutions

2.5 Optimization of Sensor Configurations

When dealing with positioning systems, such as USBL, it is necessary to deploy sensors in the vehicle that is intended to locate a transmitter emitting acoustic signals. Therefore, it is considered that four hydrophones are needed to measure the time difference of arrival of a received acoustic signal so its direction can be calculated. These hydrophones can be located anywhere along the boy of a vehicle, so it is essential to understand how can the sensor layout be designed, namely in terms of its physical distribution along the body of an underwater structure, in order to achieve the best possible estimation.

This section is dedicated to explore some commonly employed methodologies which evaluate the performance of sensor layouts considering determined parameters.

2.5.1 Crámer-Rao Lower Bound

The Crámer-Rao lower bound (CRLB) is a tool which analyzes the variance of a sensor configuration and determines the minimum bound it can achieve independently from the used estimator. This method assumes the usage of an efficient estimator, which is an optimal estimator for the chosen parameter, and an unbiased estimator, i.e. the real value of the parameter which is equal to the expected value.

In this thesis, it is conducted a study based on the CRLB, which is generally used to generate a *so-called uncertainty ellipse* [26] that represents the spatial distribution or the spatial variance distribution of the estimated position. The overall desired result is to find the minimum variance that is related to the chosen configuration geometry, which indicates that it is the optimal solution for estimating a certain position. This method utilizes the Fisher Information matrix (FIM) as explained next, which measures the quantity of information that can be extracted from an observation vector about a certain parameter.

In order to avoid loss of generality, it is considered a set of N sensors and a settled position for the acoustic source, defined by $s = [x_s, y_s, z_s]^T$. In addition, the position of each sensor is defined as $r_i = [x_{r_i}, y_{r_i}, z_{r_i}]$ and, consequently, the measurement of distance between each sensor and the source is defined as $d_i = ||s - r_i||$.

Thereafter, the observations vector will be formulated containing the observed times-of-arrival (ToA) of the signal from the acoustic source to each one of the hydrophones, considering their geometric position. These times contain a noise vector component, which can be approximated to a Gaussian distribution $n_i \sim \mathcal{N}(\mu, \sigma^2)$. The samples can be calculated through the expression (2.21), where it is considered an initial time of emission t_0. Additionally, c represents the sound speed underwater.

$$t_i = t_0 + \frac{||d_i||}{c} + n_i \tag{2.21}$$

After having the observations matrix, the condition to formulate the Fisher Information matrix, $I(d)$, is established which results into equation 2.22.

$$I(d) = \nabla_d t(d)^T \, \Sigma^{-1} \, \nabla_d t(d) \tag{2.22}$$

$\nabla_d t(d)$ is the gradient matrix of the observations vector regarding d_i, whereas Σ is the covariance matrix, in which the diagonal contains the standard deviation of the components of each noise vector, construed as $(\sigma_1^2, \sigma_2^2, ..., \sigma_N^2)$.

The Fisher Information Matrix quantifies the information that a certain sensor configuration can give about a position in space. Hence the goal is to obtain the maximum achievable information. By calculating the determinant of FIM it is possible to deduce the minimum *uncertainty ellipsoid* and therefore the configuration's best possible performance. Therefore, the optimal solution is given by the maximum output of the determinant of FIM.

Additionally, it is possible to detail this information by calculating the actual size of the axis that compose the *uncertainty ellipsoid*. This is achieved by calculating the square mean root of the eigenvalues of $I(d)$, which correspond to each axis size.

Therefore, the Crámer-Rao lower bound is widely used as a metric to evaluate the performance of sensor configurations. Further explanation about the methods used in a deeper exploration of the Crámer-Rao lower bound can be consulted in [26]. However, the mentioned concepts were all the necessary for the approach on this dissertation .

This same process is adopted in this dissertation. All steps specifically taken for this study are declared in section 5.3 of the present document.

2.5.2 Optimal Design and Optimality Criteria

When contemplating system designs, the optimal solution for a problem is generally a subjective matter which depends on the chosen criterion. Following this idea, we can define optimal designs as experimentally generated designs of various types of systems which are usually optimal for a targeted statistical model and are modeled by a specific optimality criterion. These criteria can be organized in four distinct groups [27]:

- **Information-based** : comprehends all criteria that are related to the Fisher information matrix $X'X$. Some of the criteria which fits into this category are A-, D-, E- and G-optimality.

- **Distance-based** : includes criteria which depends on the distance $d(x,A)$ from a point x in the Euclidean space $\mathbb{R}^p$ to a set $A \subset \mathbb{R}^p$. U and S-optimality are integrated in this category.

- **Compound design** : combine different adjusted criteria in different weighted proportions in order to meet a desired statistical function.

- Other : all criteria which do not fit in the previous three sets can be encompassed in a fourth general set.

The most relevant category for the present work is the information-based criteria, since we want to maximize the information that can be extracted from a certain design and we do not need to minimize the distances between the receptors and the source. Therefore some of the most commonly used criteria will be better explained in the following subsections, which correspond to the chosen metrics for optimizing the localization precision during the present research work.

2.5.2.1 A-optimality

The A-optimality criterion intends to minimize the trace of the inverse FIM, i.e. the mean-squared error (MSE) [28]. This corresponds to minimizing the summed eigenvalues of the FIM, which correspond to the length of the uncertainty axis, denoted as (2.23).

$$min(\ trace(I^{-1})) \tag{2.23}$$

In applications where it is desirable to achieve a balanced uncertainty estimation in all directions, the A-optimality can lead to misleading conclusions as it can disguise larger uncertainty magnitudes in a single direction.

2.5.2.2 D-optimality

The D-optimality criterion minimizes the volume of the uncertainty ellipsoid associated with a specific estimate [29]. This is achieved by maximizing the FIM determinant, which maximizes the information that is possible to be obtained for a specific estimation. Alternatively, it can also be described as intending to minimize the determinant of the inverse FIM, (2.24), which corresponds to minimizing the ellipsoid uncertainty volume. This metric is widely used to achieve an optimal sensor geometry for single target estimation and 2D sensor placement.

$$min(\ det(I^{-1})) \tag{2.24}$$

This criterion presents advantages comparatively to other criteria, namely it is invariant under parameter scale changes and linear transformations of the output However, this optimization criteria can be misleading since a determinant value that is minimal can be disguising an ellipsoid uncertainty axis that is much larger than the remaining for the same estimate [28], leading to a disproportionate estimation precision that it intended to be avoided.

2.5.2.3 E-optimality

The E-optimality criterion intends to minimize the maximum eigenvalue of the inverse FIM, i.e. minimizes the larger ellipsoid uncertainty axis corresponding to direction with the worse estimation precision. Expression (2.25) [27] denotes this condition, where λ_{max} is the maximum eigenvalue of the inverse FIM.

$$\lambda_{max}(I^{-1}) \tag{2.25}$$

Although this criteria is mitigating the worse ellipsoid uncertainty direction, it does not take into account the entirety of the ellipsoid uncertainty volume. It is usually the preferred criteria in applications where it is necessary to have a more homogeneous estimation precision in all directions, such as for approximation of objects that should not collide.

As the present dissertation considers a scenario that requires the approximation of AUVs, which would to be preferably placed within few centimeters from each other, the E-optimality is considered the most relevant throughout the results analysis of this research work.

2.5.3 Particle Swarm Optimization

The Particle Swarm Optimization (PSO) is a Swarm Intelligence based computational method, which iteratively improves the candidate to a solution of a problem through cost functions. It is based on the behavior of environment entities (particles), such as fish schools or flocks of birds, and it approximates a candidate to the optimal solution by moving each particle in the direction of its previously best position (*pbest*) and the global best position (*gbest*) [30].

Given the standard algorithm for the PSO, equation (2.26) expresses the velocity V_i of the particles movement, which can be limited to avoid that particles fall of the intended region, and (2.27) is the position P that is updated. Additionally, the t corresponds to the current iteration number, i is the particle index, w denotes a inertia weight that balances the global and local exploration, c_1 and c_2 are acceleration coefficients and r_1 and r_2 are random variables uniformly distributed withing the range [0,1].

$$V_i(t+1) = wV_i(t) + c_1r_1(pbest(i,t) - P_i(t)) + c_2r_2(gbest(t) - P_i(t)) \tag{2.26}$$

$$P_i(t+1) = P_i(t) + V_i(t+1) \tag{2.27}$$

A comprehensive survey on PSO algorithm adaptations and common applications is presented in [30], which include optimization of sensor localization for estimation improvement.

In this regard, article [31] explores the use of PSO to determine an optimal receiver configuration for Short-Baseline localization, which corresponds to a similar application to the conducted research in the present dissertation. In this study, a single transducer is placed on an AUV and four receivers are mounted on a mothership. The position estimation is based on the

Euclidean distances between the transmitter and the receivers. After applying the PSO it is concluded that the optimal configuration achieved is different than the initially expected, leading to a 6.64% improvement on estimation precision.

Chapter 3

Research Problem

This chapter intends to clarify the problem addressed by the present dissertation. Section 3.1 presents the details behind the research work as well as the problems it intends to solve. Having this clear, the dissertation hypothesis is stated in section 3.3 along with the research questions that are the main issues that are being explained with the present document. Lastly, the used validation methods are specified in section 3.4.

3.1 Problem Statement

The Ultra-Short Baseline system is among the most deployed positioning methods using underwater acoustics. There is a vast knowledge of its function and capabilities, therefore its implementation does not constitute a technological innovation nowadays. In the considered scenario, previously mentioned in chapter 1, an AUV is taking part on a long-term underwater mission in which it periodically sends known signals to the surface with a pinger. In such case, the mule AUV needs to be provided with an USBL system to receive the signal and estimate the position of the other AUV to navigate near it. The simplified communication system is illustrated in figure 3.1.

This partial USBL system was developed in previous dissertations and research work, which can be better understood in [32]. Briefly, the system consists on a transducer of four hydrophones forming a 3D array deployed on the mule AUV. The distance between AUVs is given by the cross-correlation between the received and expected signals. Since the operation frequency range is around tens of kilohertz, which minimizes the attenuation of sound, the time difference of arrival has to be refined by analyzing the relative phase differences between hydrophones.

Considering that the survey AUV navigates freely trough unknown locations, the USBL system to be employed needs to fulfill particular requirements that common commercial solutions do not comply.

Firstly, the system needs to be able to cover both short and long range distances, going from tens of centimeters to several hundreds of meters between the receiver and the transmitter, with the best estimation precision possible. For long range positions, the accuracy of the estimation

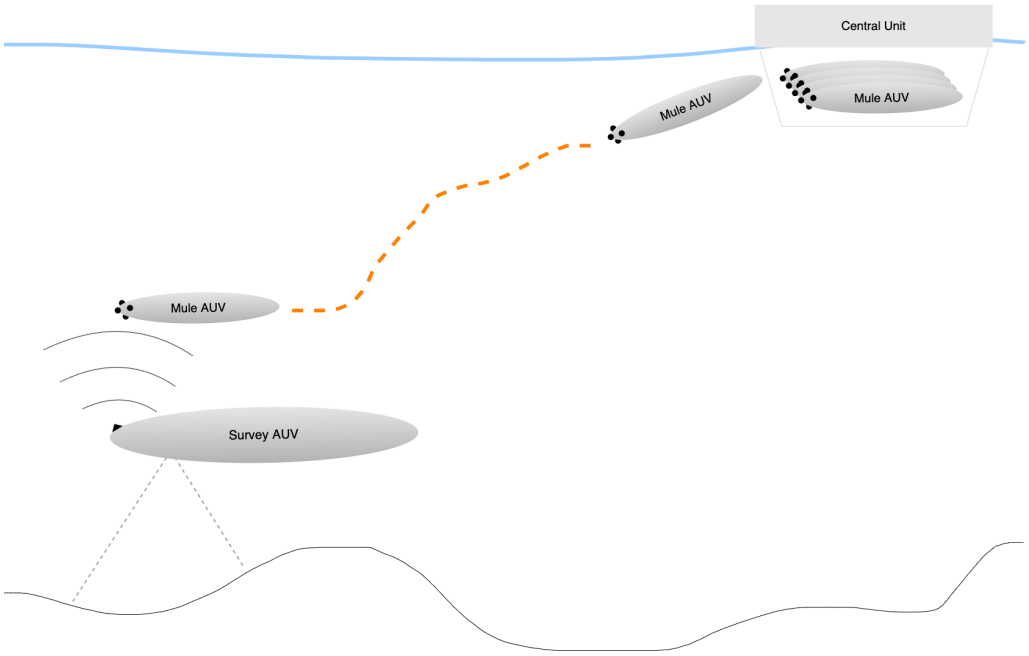

Figure 3.1: Context of the GROW project

affects how direct is the path for the mule AUV to reach the acoustic source. This influences the overall energy consumption, duration of navigation search and can affect the reliability of the process. For short range position, an accurate estimate allows to avoid collisions and correctly establish chosen relative positions between vehicles. Additionally, an increase in the frequency of position estimation would consume more power but provide more robust positions, which is desirable for short range scenarios. The available market systems usually offer multiple solutions with different limited operation ranges, which would force to employ more than one system to achieve the mentioned range requirement.

Secondly, the USBL system needs to be capable of detecting incoming signals from any position in space, since the localization detection is solely based on the received signals. Since the system is composed by various sensors, it is expected that they are arranged in varied positions and with different perspectives so they can cover a wider area. However, considering they are supposed to be employed on an AUV, the vehicle's body represents an opaque obstacle to signals. Therefore, with only four fixed hydrophones, it is not possible to detect positions with full line of sight, as intended, since not all hydrophones would have line of sight to the transmitter at all times.

The system that is proposed in this dissertation intended to resolve this technological gap with a system that satisfies the described requirements. Since only four hydrophones are enough to obtain a position estimation (bearing and distance), if they assume a fixed position on an AUV's body it would inevitably limit the direction to where the sensor has direct line of sight. Therefore, the suggested method implies deploying multiple sensors in the vehicle. From the available sensors, only four would be used simultaneously to receive the signals and feed them

to the processing system. By adopting this concept, a main issue that arises is where to place the hydrophones within the vehicle. This constitutes the main research topic conducted in the present thesis.

Considering that the mentioned mechanism is meant to be applied in mobile vehicles with changing environment conditions, it is useful to integrate it in a system which is responsive in real time. Accordingly, the process that selects four hydrophones among the available set can be transformed into a dynamically reconfigurable system which enables the hydrophones commutation according to the sensors' configuration that minimizes the estimation error.

The study conducted in the scope of this dissertation intends to prove the functionality of the developed method, validate the hypothesis declared in 3.3 and draw conclusions on the research questions.

3.2 Assumptions

This research work relies on a set of premises that were considered throughout the development of the proposed system, as presented in this section.

Number of sensors For the estimation of the position in 3D space, a multilateration approach was used, as explained in 2.2.2.2. Therefore, a minimum of 4 hydrophones are needed so that it is possible to define the position of the transmitter. Using only two sensors, two possibility spheres are formed around these sensors whose intersection originates a circle that contains the location possible solutions. By adding a third sensor, this circle is intersected by another sphere which originates only two location possibilities. Finally, a fourth sensor is added to exactly differentiate which is the accurate location solution.

Synchronism The system integrates a synchronization mechanism that allows to know the time of emission of an acoustic signal and Hence it is possible to compute the ToA of the signal which indicates the range between the transmitter and the receiver.

Noise characteristics The system assumes an injected error e_i added to the time differences of arrival, Δt_{ij}. These errors are mutually independent and follow a Gaussian distribution with zero mean and a configurable variance of σ^2, i.e., $e_i \sim \mathcal{N}(0, \sigma^2)$.

For the simulations performed in this project, a deviation of 5°, or a window of $[-2.5^\circ, 2.5^\circ]$, in phase difference estimation of incoming signals was considered to be reasonable for an underwater navigation scenario. Therefore, since the specified period of the signals is $T = \frac{1}{24400}$, then the 5° will be equivalent to $\frac{5^\circ}{360^\circ} * T$ which is approximately a deviation of $0.5\mu s$. Hence the considered standard deviation σ of the error e_i in the computed time differences of arrival is equal to $0.5\mu s$.

Numeric quantization The digital signal processing system uses a finite quantization resolution with 7 decimal places for the phase difference. Since the added noise expressed in degrees is an

integer, which is 10^7 times larger than the system resolution, then the numeric quantization is not significant in the present work.

Reference axis The origin of the reference axis is defined at the center of the structure where the hydrophones are fixed, which in this case is the AUV.

Propagation speed The considered speed of sound is 1500 m/s, which corresponds to the underwater propagation velocity of waves in typical conditions.

3.3 Hypothesis and Research Questions

This dissertation intends to complement previous research work and answer to a core research hypothesis which serves as fundamental investigation purpose. This research hypothesis can be stated as:

"Using a USBL system that reconfigures the hydrophone selection leads to an improvement on the underwater localization precision, allowing to always have a set of four active hydrophones with line of sight to the transmitter and makes it suitable for both short and long range estimation."

Attending the proposed hypothesis, the topics that are intended to be explored and discussed in this thesis's work can be summarized in the following research questions:

RQ1: *What method should be adopted in order to efficiently compare the performance of hydrophone configurations?*

RQ2: *What decision metric(s) should be used to evaluate the optimal hydrophone configuration for a specific angle of arrival?*

RQ3: *How should the system be developed in order to assure that the selected hydrophones always have line of sight to the transmitter?*

RQ4: *Are there distinct best hydrophone configurations for short and long range estimation?*

These questions summarize the main topic points which are explored in the scope of this thesis and are the essential inquiries that it intends to answer.

3.4 Validation Methods

The validation of scientific work is a key factor to demonstrate how reliable and effective it is. In this thesis, three essential methods are used to validate the functionality of the developed techniques:

- **Simulation**

  The considered immediate approach to evaluate the functionality and behavior of the system consists in creating a set of simulation procedures which are as close as possible to the real environment and the physical system. These simulations were made as MATLAB scripts carefully designed to integrate realistic parameters, such as expected environment noise and other limitations.

- **Scientifically recognized methods**

  When composing a system, it can be useful comparing the studied approach with widely used methods which are recognized in the scientific community. By doing this, we can gain a level of confidence in the developed system and in the obtained results.

- **Field experiments**

  After having the analytical methods and simulations coherent, it is essential then to test the system in a real environment in order to assess the functionality and performances when real conditions are added. By testing it in a real application it is possible to take conclusions about its robustness and consider improvements or refinements for the system. Due to the exceptional pandemic situation, in the present work it was only possible to perform field tests on the developed digital signal processing module.

Chapter 4

Digital Signal Processing

To implement the USBL system, a custom digital signal processing system has been implemented to compute in real-time the time differences of arrival of the acoustic signal arriving to the hydrophone array. The system was implemented in a FPGA-based platform and included in a previous signal processing system that determines the time of arrival of an encoded acoustic signal by implementing an efficient time-domain cross correlation.

This chapter introduces the process to calculate the time differences of arrival by combining the results of the cross-correlation with the differences of phase between the signals received by the different hydrophones.

4.1 TDoA Estimation

To improve the determination of the time difference of arrival between the hydrophones, the implemented signal processing system calculates the difference of phase between the received signals. As the distance between hydrophones, i.e. the baseline, is always larger than the wavelength of the acoustic signals used, the phase alone is not sufficient to determine the time difference of arrival. Time-domain correlation is thus combined with the phase difference calculation to remove the ambiguity and obtain a time difference of arrival with a time resolution that is far beyond the sampling period used in the digital signal processing system.

When the information about the time of arrival of a signal is available, it is relatively easy to estimate the distance between the transmitter and the receiver since there can be a direct conversion between them. However, when dealing with phase differences, there is no exact time notion, so it is necessary to start by defining a reference point.

Considering sinusoidal signals, when we have an array with four hydrophones spatially placed to form a 3D layout, the signal that is arriving to each hydrophone in different times consequently have different phases. However, since sinusoidal signals are periodic, this means that for different signal periods the same phase value is observed, i.e. the phase is ambiguous 4.1. In this illustration, α represents the observable phase difference of hydrophone H_4 to the

reference point H_1. However, the actual time difference which is intended to obtain, Δt_4, is one period of the signal, λ, added to the observable phase α.

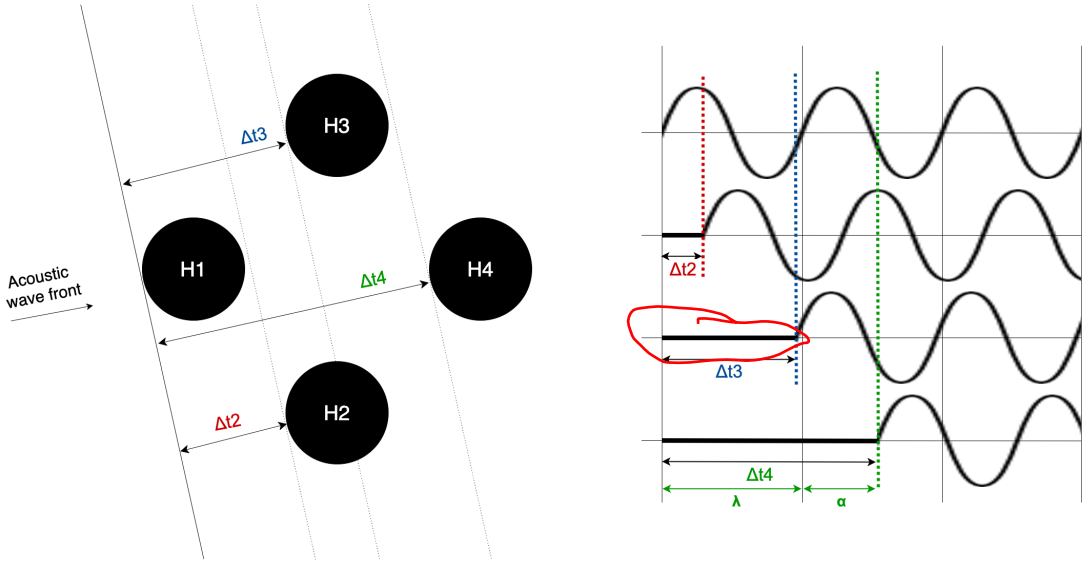

Figure 4.1: Phase difference to reference point and phase ambiguity

For this reason, it is crucial to consider that the phase difference is given by the obtained phase value added by the number of periods ahead from the considered reference period.

In the system under study, the transmitted signal is a pure sine wave with a frequency of 24.4 kHz. The corresponding signal period is $T = \frac{1}{24400}$ seconds which, considering the typical underwater acoustic speed c_s equal to 1500 m/s, the wavelength is approximately equal to $\lambda = \frac{T}{c_s} = 6.1cm$. Having this into consideration, after obtaining the time of arrival to each hydrophone given by the cross correlation instances, besides the reference one, it is possible to conclude if the phase shift is superior to one period by analyzing if the time difference is greater than the duration of one period T. In figure 4.1, each mentioned time difference Δt_2, Δt_3 and Δt_4, between H_1 and H_2, H_3 and H_4 is converted to the corresponding phase differences.

One possibility to solve phase ambiguity in this system would be to place the four hydrophones with a baseline spacing inferior to $\frac{1}{2}$ of a wavelength, since the maximum reached by phase difference is 180 degrees. This way it would be possible to immediately deduce the phase difference since it would always be contained in one period. However, positioning the hydrophones closer together leads to smaller values, causing an increase on the estimation error due to varying environment conditions (briefly enumerated in 2.1). Additionally, since the hydrophones to be used in this system have a corresponding diameter of roughly half of a wavelength, they would not allow to execute the mentioned configuration and so this possibility will not be contemplated.

In order to compensate this phase ambiguity, a simple relation was developed which allows to calculate the absolute time difference between the moment a signal is received by hydrophone A, T_A, and when the same signal is received by a further hydrophone B, T_B. Figure 4.2 illustrates

this association, where the represented sinusoidal waves correspond to the same signal arriving at hydrophones A and B.

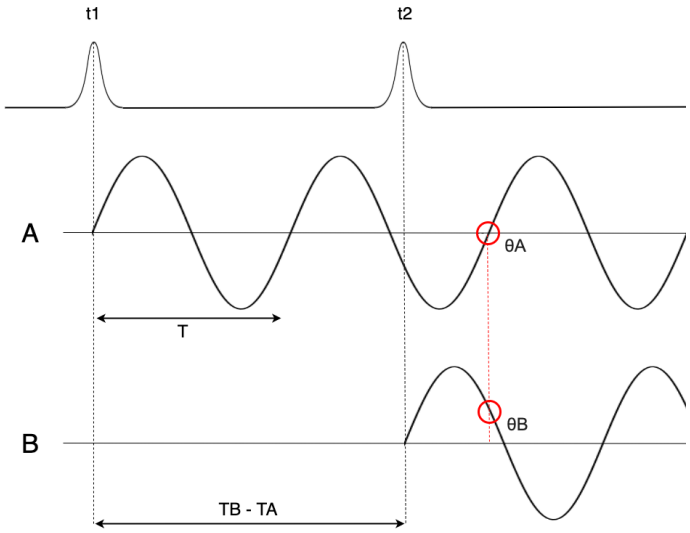

Figure 4.2: Ambiguity correction through correlation and phase difference

This correspondence uses the time stamps obtained by the correlation peaks combined with the calculated phase difference, that is determined in parallel, so that the measurement is more accurate. Equation (4.1) translates this relation, where t_1 and t_2 are the correlation peaks obtained from the signal arriving at hydrophone A and B, respectively, and so by rounding for the next integer number the difference between the correlation peaks, $t_2 - t_1$, we will obtain in which period, T, of signal in A will the signal in B arrive. Then the measurement is improved by subtracting a phase difference, $\theta_B - \theta_A$, so that the instant at which the signal is detected in hydrophone B can be defined.

$$T_B - T_A = round(\tfrac{t_2 - t_1}{T}) - (\theta_B - \theta_A) \tag{4.1}$$

4.2 HDL Module Architecture

In a previous dissertation project [32], a signal processing system has been implemented to determine the time difference of arrival of an acoustic signal to a set of 4 hydrophones. This system is based on the transmission of a known binary sequence modulated in PSK (Phase Shift Keying) and the detection of the signal received by performing an efficient time-domain cross-correlation between the signals received at each hydrophone and the transmitted signal. The system was intended to determine the 3D position of an acoustic source in a confined structured space, where the 4 hydrophones were distanced a few meters between them. The implemented correlation process allow to obtain the time of arrival of the sound wave with a timing resolution equal to one

sampling period that corresponds to a distance resolution approximately equal to 6 mm, which has been considered enough for the spacial accuracy of the 3D positioning system.

The current work intends to enhance that system to improve the accuracy of the calculation of the time differences of arrival. This is achieved by computing in real time the phase differences between the signals arriving to each hydrophone and combining that with the time of arrival calculated by the correlation process. The objective of this system is to implement a Ultra-Short Base Line (USBL) underwater localization system to estimate the 3D angle of arrival of the acoustic signal, for integration in a small Autonomous Underwater Vehicle (AUV). Due to the relatively small size of the AUV, the 4 hydrophones will have to be separated by the maximum of a few tens of centimeters. Therefore, the maximum resolution in distance that is possible to obtain with the correlation process alone is not enough for accurately determining the angle of arrival. Preliminary experimental results have showed that, with the phase analysis combined to the cross-correlation, the time differences may be obtained with an accuracy corresponding to a distance below one millimeter.

To implement this process, that acoustic source transmits a sinusoidal signal with a know fixed frequency (24.41 kHz) after the BPSK encoded signal used by the correlation process. The phase analysis mechanism makes use of this signal which is know to appear a fixed time after the detection of the encoded signal.

4.2.1 Module Components

The overall system is composed by four main functional blocks, represented in 4.3. The hydrophone array, composed by hydrophones i with $i = \{1,2,3,4\}$, receives the signals in each sensor and sends them to an Analog to Digital Converter (ADC). The generated digital signals are then input of a module based on a Hilbert transform, which converts the real signals to their complex representation. These are then multiplexed so each pair of real, Re_i, and imaginary, Im_i, components are input in a CORDIC [33] block, responsible for computing the signal's phase, $phase_i$. Afterwards, the phase differences $phdiff_{ij}$ are calculated for all the combinations of two hydrophones and finally they are averaged in order to obtain a more stable phase difference, $\Delta phase_{ij}$.

The module receives a global clock and reset which are connected to all registers, as well as an enable signal which allows the sub modules to capture new inputs and release the outputs synchronically.

The sampling frequency of the input signals is 244 kHz and the whole digital circuit works with a global clock signal equal to 125 MHz. Thus, there are 512 clock cycles available between each two arriving signal samples and, as the calculations to perform are simple, these are more than enough to originate the outputs, therefore this architecture does not involve time constraints. Instead, it focuses on minimizing the used area since it is part of a complex system that already uses a substantial part of the FPGA resources.

In order to describe the efforts to minimize the used area, all module sub components are detailed next, namely the Hilbert filter, CORDIC, Phase difference and Mean phase.

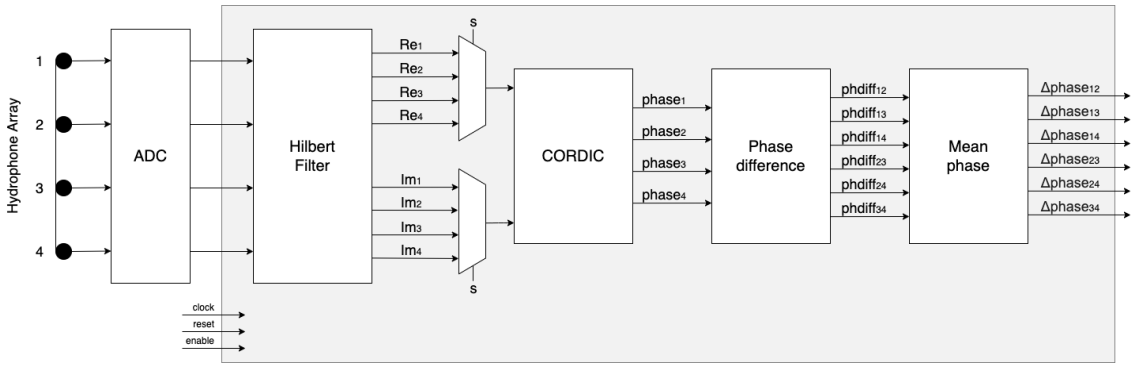

Figure 4.3: Top level architecture

4.2.1.1 Hilbert Filter

The signals coming from the ADC are purely real so they need to be converted to their analytic representation. This is achieved by using a module based on a Hilbert FIR filter, which derives the complex representation by comprehending the original real signal and its Hilbert transform.

The Hilbert transform definition is given by (4.2) [34], where $x(t)$ is the original signal and P is the Cauchy principal value.

$$H(x)(t) = \frac{1}{\pi} P \int_{-\infty}^{\infty} \frac{x(\tau)}{t-\tau} d\tau \tag{4.2}$$

An 8-th order Hilbert FIR filter was designed using the Matlab function *designfilt* and has only 4 non-zero coefficients. Although this will provide an inaccurate calculation for the instantaneous phase of the input signals along the signal period, it has been observed with Matlab simulations that this approximation will be enough for obtain an averaged phase difference within a few degrees. Nevertheless, the length of the Hilbert filter can be easily increased without a significant impact in the digital design complexity.

Having the 4 non-zero filter coefficients $a_k, k = 1,...,7$, that respect an odd anti-symmetry, i.e. $a_1 = -a_7$ and $a_3 = -a_5$, the imaginary and real components of the input signal x_i are obtained by following equations (4.4) and (4.4).

$$Imag_0 = a_1\, x_{-1} + a_3\, x_{-3} + a_5\, x_{-5} + a_7\, x_{-7} \tag{4.3}$$

$$Real_0 = x_{-4} \tag{4.4}$$

In order to implement this filter, the most common approach is to use a chain of registers that integrate multiple adders and multipliers, so that the calculations take less clock cycles to obtain a valid result, similarly to the work in [35]. However, since the goal of this implementation is to minimize area, then an alternative approach was formulated which uses only one multiplier and one adder. As can be observed in the filter equation, all odd samples need to be multiplied by a

coefficient and summed with each other. Therefore, by using a circular shifting register chain 4.4 for each arriving signal, it is possible to position each of the buffer chain's samples in register x_8, which is used for external calculations.

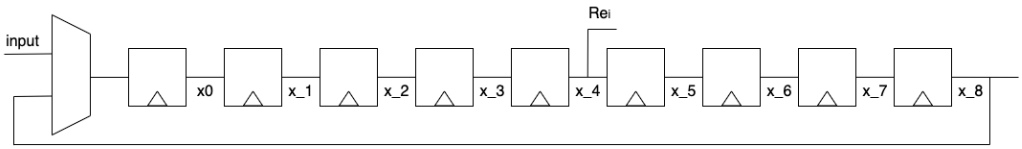

Figure 4.4: Hilbert Filter circular shifting register chain

In a more comprehensive view, the register chains HF_{Ci} are integrated with the remaining block elements as represented in 4.5. The four shift-register chains receive four signals as input and output the real and imaginary components, $Real_i$ and $Imag_i$, for each of them.

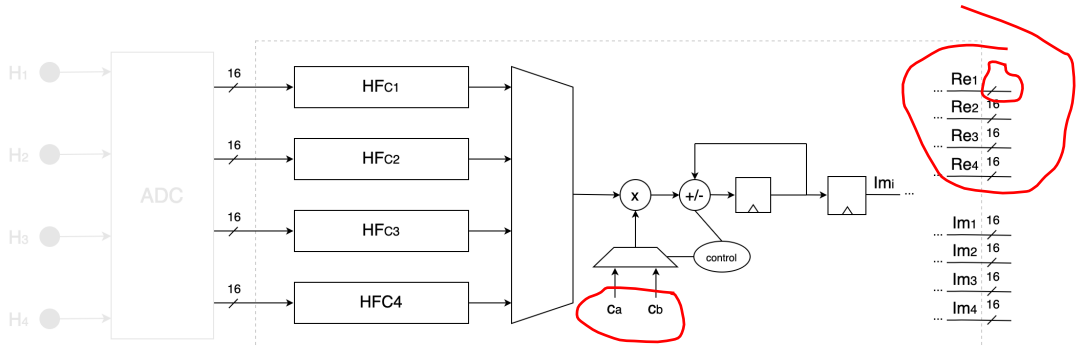

Figure 4.5: Hilbert Filter block diagram

The implementation contains a series of design decisions that lead to decreased area occupation, presented as follows :

- The four register chains are multiplexed so that the module needs only one multiplier and one adder to calculate the Hilbert transform for all signals;
- Since the coefficients have odd symmetric pairs, then only two variables and their symmetric value are needed, which will be referred as c_a, c_b, -c_a and -c_b. For even samples, associated with coefficients equal to zero, a controller unit is responsible for skipping the multiplication, which saves energy. For odd samples, the control unit alternates between the positive and negative coefficients to be multiplied. The control unit settings are summarized in table 4.1 for each register chain sample.
- The negative coefficients are achieved by subtracting the result of $a_i\ x_{-i}$, i.e. negating the adder, so only one adder block is necessary;
- A register is placed after the adder so that it interactively accumulates the value that is correspondent to the imaginary component Im_i after the full chain circle shifting.

	Multiplier Coefficient	Adder mode
a_0	0	-
a_1	-c_a	-
a_2	0	-
a_3	-c_b	-
a_4	0	+
a_5	c_b	+
a_6	0	+
a_7	c_a	+
a_8	0	+

Table 4.1: Hilbert filter control unit settings for each processed sample with $c_a = 0.23932$ and $c_b = 0.62610$

Having cleared the implementation details, it is possible to deduce that each HF_{Ci} takes 9 clock cycles to be processed. Therefore, the entire calculation of the complex representation of the four input signals takes 9×4 clock cycles plus one additional cycle to update the outputs.

4.2.1.2 CORDIC

The CORDIC algorithm is used for real-time trigonometric and exponential calculations, as well as polar to rectangular conversions and vice-versa, using iterative vector rotations.

The implemented CORDIC module has a sequential structure, as it occupies the least area, and it is responsible for receiving the real and imaginary components of a signal and calculating its phase. There are two possible modes of operation from which it is used the vectoring mode (VM), whose algorithm computes the magnitude and phase of the input vector (x_0, y_0) from the x-axis [33]. This is achieved by iteratively approximating the phase through angle microrotations of $\alpha_i = \pm atan(2^{-i})$ which are summed originating an approximated phase. The result is given in a 16 bit value, which is composed by 9 bits for the integer part and 7 bits that represent the fractional portion.

The CORDIC iterations are expressed by (4.5), (4.6) and (4.7) for d_i belonging to {-1,1}.

$$x_{i+1} = x_i - d_i \, 2^{-1} \, y_i \tag{4.5}$$

$$y_{i+1} = y_i + d_i \, 2^{-1} \, x_i \tag{4.6}$$

$$z_{i+1} = z_i - d_i \, \alpha_i \tag{4.7}$$

The CORDIC logic uses a 16 element ROM (Read-Only Memory) that stores the $atan(2^{-1})$ values required for the algorithm. Additionally, another sub component provides a binary counter

that defines the number of performed iterations and it is also responsible for generating the address to access the ROM.

Considering that the CORDIC module uses 16 clock cycles to run through the entire ROM and one additional cycle to update the outputs. Therefore, the design uses only one CORDIC module with multiplexed inputs so the process takes 17×4 plus one, to update the global outputs, in a total of 69 clock cycles.

4.2.1.3 Phase Difference

This sub module is responsible for computing the phase differences between the previously determined signals' phases, $phase_i$. For four inputs $phase_i$, it is generated the difference between all pairs of different hydrophones, h_i, h_j, h_1,h_2, h_1,h_3, h_1,h_4, h_2,h_3, h_2,h_4 and h_3,h_4.

This is achieved using a single subtractor which has multiplexed inputs so that the calculations can be executed within the 512 clock cycles with only one block of hardware, instead of dedicated subtractor for each calculation.

The result is given in a 16 bit value, which is composed by 10 bits for the integer part and 6 bits that represent the fractional portion.

4.2.1.4 Mean Phase

Finally, the last module implements a moving window averaging filter, with a window size $N = 2^k$ configured by the parameter k, with values from 1 to 6. The final averaged phase differences are in the range [-180º,+180º], represented in 16 bits with 7 bits for the fractional part.

4.2.2 Implementation Results

The design was synthesized to a XILINX XC7010 Zynq device and integrated in the digital signal processing system implemented in a Red Pitaya platform. Although this block is only a part of a more complex signal processing system that also includes the correlation calculators as described in [32], it occupies only 1216 flip-flops and 1462 Look-up tables, which represents a small fraction of the available FPGA resources. Besides, the sequential implementation of the Hilbert FIR filter and CORDIC module and the sharing of the modules among the four input signals has reduced the size of a previous preliminary implementation which used more than 10k flip-flops and 6k Loop-up tables.

4.3 Doppler Effect

The implemented process uses the information of the transmitted signal's operating frequency in order to compute the phase differences and determine the overall times of arrival. However, in real scenarios the environmental and the operational conditions will distort the frequency perceived by the receiver due to the relative movement between the acoustic source and the receiver.

In order to evaluate if the Doppler effect influences the system, it is possible to calculate the frequency deviation observed for a known relative speed between vehicles. Considering that the relative speed between the transmitter and the receiver is denoted as $relative\_speed$ and using a fixed sound speed, c_s, with a determined frequency of the transmitted signal, the relation (4.8) can be established.

$$freq\_deviation = \frac{relative\_speed}{c_s} \times signal\_freq \tag{4.8}$$

Therefore, considering a maximum relative velocity between the transmitter and the receiver equal to $\pm$ $5m/s$, this will impact in a frequency deviation perceived by the receiver equal to $\pm$ $81Hz$, which corresponds to a relative error of 0.33% of the nominal frequency and approximately the same relative deviation for the period of the signal reaching the receiver. As the time differences calculated from the phase differences are directly proportional to the expected signal period, concerning the calculation of the time difference of arrival to different hidrophones, the Doppler effect has been considered negligible.

A way to prevent this deviation is to integrate a frequency detector which senses the relative navigation speed in real time and adapts the used frequency. This mechanism is not integrated in the present research work.

Chapter 5

Sensor Configuration Performance Evaluation

As previously declared, the present dissertation ultimately intends to develop a reliable method that determines the optimal configuration to minimize the estimation error. For this purpose, it is necessary to employ a complementary mechanism which is able to perform experiments on sensor configurations in order to quantify their performance based on chosen decision parameters.

Therefore, three different methods will be presented in this section as potential tools to be used. Firstly, a theoretical approach will be detailed, followed by a functional exemplification of each process. Lastly, a practical comparison between them will be presented in order to disclose the preferred option for this application. The first two methods are based on the estimates dispersion given by Monte Carlo simulations of a position estimator, namely a geometry based estimator based (GBE) and an estimator that assumes a plane wavefront (PWE), while the third is based on the Fisher Information Matrix.

For all methods, the same scenario is considered which is illustrated in 5.1. It is assumed four hydrophones placed in known relative positions in space and the origin of the axis is set on the body of the AUV or an alternative fixed structure. Then r_i is defined as the vector that connects the origin of the axis to hydrophone i and rr_i defines the vector that connects hydrophone i to the acoustic source. The black cross represents the acoustic source which is located somewhere in space. At last, the subtraction of the mentioned vectors is equal to r, according to (5.1), which corresponds to the position of the acoustic source in relation to the origin of the axis.

$$r_i = r + rr_i \tag{5.1}$$

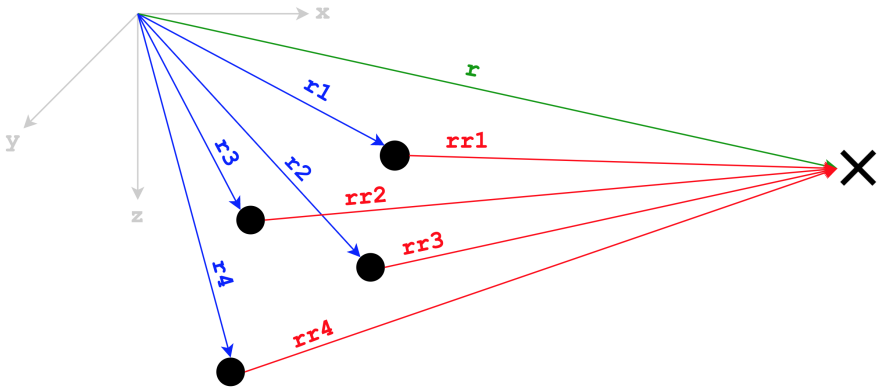

Figure 5.1: Considered scheme for angle of arrival estimation

5.1 Geometry based Position Estimator

The goal of the first proposed method is to estimate the position of an acoustic source in relation to known positions of a configuration of sensors, in a system of geometric axes with a defined origin. For this purpose, the logic employed is based on vector algebra with other physical considerations, detailed in the present subsection.

Considering the presented scenario in 5.1, this explanation starts by defining the times of arrival to each hydrophone as (5.2). t_0 is the absolute time of emission, c_s is the underwater sound speed and ρ_i is the norm of rr_i, (5.4), which translates to the distance from hydrophone i to the acoustic source.

$$t_i = t_0 + \frac{\rho_i}{c_s} \tag{5.2}$$

However, instead of computing the absolute ToA of each hydrophone with (5.2), they can be expressed as a function of a single reference ToA, which allows to rely less on the synchronization mechanism. Therefore, for two sensors with known relative positions, the time of arrival from a transmitter to hydrophone j is given by a reference time of arrival, t_i, added by the time difference of arrival Δt_{ij} (5.3) and an injected error e_i according to 3.2.

$$t_j = t_i + \Delta t_{ij} + e_i \tag{5.3}$$

A simple logic was applied in order to determine the mentioned reference hydrophone, which starts by identifying the closest to the acoustic source. This allows to obtain all relative times of arrival by adding the defined reference time to each TDoA between a hydrophone and the reference one, Δt_{ij}. This is achieved by analyzing the of each pair of possible combinations of two among four hydrophones, making up a total of six combinations. Considering each hydrophone pair ij with $i, j = \{1,2,3,4\}$:

- if Δt_{ij} is positive, then hydrophone i is closer to the acoustic source
- if Δt_{ij} is negative, then hydrophone j is closer to the acoustic source
- if Δt_{ij} is zero, then i and j hydrophones are equidistant to the acoustic source

Considering these relations, it is possible to compose a vector that accumulates the closer hydrophone between each pair for a certain position of the acoustic source. Extracting the mode of this vector will then return the chosen hydrophone in most cases and therefore the overall closer to the acoustic source. If the closer hydrophones are the equidistant to the source, then it is indifferent which one is selected.

If then the distance ρ_i is raised to the power of two, we know that $||rr_i||^2 = r_i^T r_i$, which allows to deduce equation (5.5) after some mathematical manipulation. Considering ρ_i a physical distance, it is also possible to express it trough equation (5.6), which uses the speed of propagation underwater multiplied by the ToA of the signal from the acoustic source to hydrophone i.

$$\rho_i = ||rr_i|| \tag{5.4}$$

$$\rho_i^2 = r^T r + 2r^T r_i + r_i^T r_i \tag{5.5}$$

$$\rho_i^2 = c_s^2 (t_i - t_0)^2 \tag{5.6}$$

Since two distinct relations are defined for ρ_i^2, then it is possible to consider the algebraic expressions as equivalent, thus forming a single equation to be resolved with only one unknown variable. After some mathematical manipulation, the matrix relation 5.7 is achieved, where r is isolated and can be estimated.

$$\begin{bmatrix} 1 & 2r_i^T \end{bmatrix} \begin{bmatrix} r^T r \\ r \end{bmatrix} = \begin{bmatrix} c_s^2 (t_i - t_0) - r_i^T r_i \end{bmatrix} \tag{5.7}$$

In order to resolve this system of equations and isolate r, the least squares method is applied. If (5.7) is extended to the four considered hydrophones, we obtain matrix A represented as (5.8) and Y equivalent to (5.9). It is important to notice that $(A^T A)$ has to be invertible, thus the rows which contain the chosen hydrophone configuration have to be linearly independent. The least squares method is then expressed as (5.10), where $X \in \mathbb{R}^4$ holds the Cartesian result of r. As the method formulates four equations that are meant to calculate only three coordinates, X will contain a fourth element that consists on a nonlinear component equivalent to $||r||^2$.

$$A = \begin{bmatrix} 1 & 2r_i^T \end{bmatrix} \tag{5.8}$$

$$Y = \left[c_s^2 \left(t_i - t_0\right)^2 - r_i^T r_i \right] \tag{5.9}$$

$$X = (A^T A)^{-1} A^T Y \tag{5.10}$$

After inferring the Euclidean vector r, it is possible to obtain both the bearing trough its direction, $\hat{r}$, and the range through its magnitude, $||r||$.

5.2 Plane Wavefront based Position Estimator

The second explored method for evaluating sensor configurations' performance is a simpler approach than the previously proposed. It consists on an estimator which assumes that the signals' propagation can be approximated by a plane wavefront. When considering a plane wavefront approximation, it is assumed that the acoustic source is at a distance which is sufficiently larger than the relative distances between the hydrophones for the planar wavefront approximation to be adequate, thus the angle of arrival to each hydrophone being the same. This estimator is posteriorly integrated in a Monte Carlo approach to evaluate the configurations based on the obtained variance given different acoustic source positions.

Using a plane wavefront approximation means that, for signals arriving to the USBL system, it is assumed that the wavefront is coincident with a plane perpendicular to the direction of propagation, thus perpendicular to the angle of arrival as well. Figure 5.2 is illustrative of a plane wavefront arriving at two sensors. As represented, knowing the angle of arrival is considered the same for every sensor, since the wavefront is the same, it is possible to deduce the time of arrival to an hydrophone 1 by using the ToA to hydrophone 2 added by the time difference of arrival between 1 and 2. Under the assumption that at least four non-coplanar hydrophones can detect the time of arrival, the inverse problem is solvable.

The estimator considers a USBL system composed by four sensors whose positions are previously defined. The time of arrival, t_i, to each hydrophone, i, is represented by expression (5.11). The considered t_0 is the absolute time of emission of the signal, which is acquired through a synchronization mechanism, the s is the position of the transmitter, a is referent to the mass center of the USBL's position, r_i is the Cartesian coordinates of the hydrophone's position, c_s is the sound speed and e_i is an injected error that have the same characteristics expressed previously in 3.2.

$$t_i = t_0 + \frac{||s-(a-r_i)||}{c_s} + e_i \tag{5.11}$$

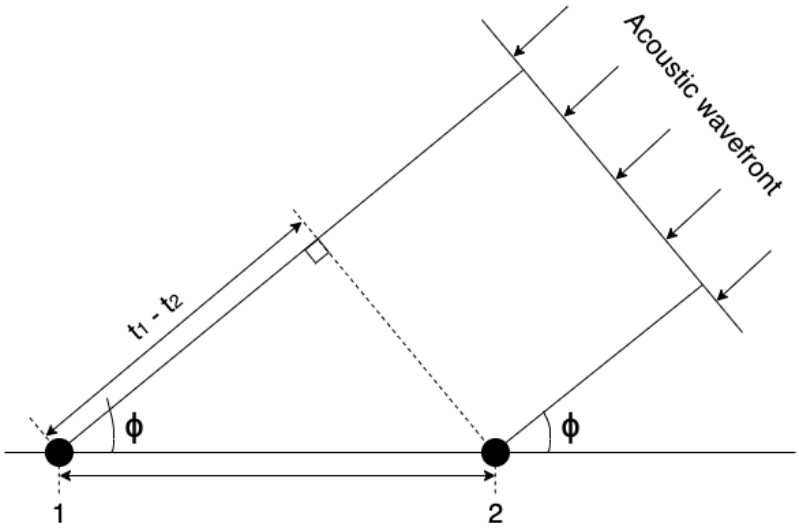

Figure 5.2: Angle of arrival relation considering a plane wavefront

Due to the considered approximation to the plane wavefront, it is possible to calculate the range estimation, ρ, as a mean all propagation times multiplied by the sound speed, c_s, as in equation (5.12). The N represents the number of hydrophones.

$$\rho = c_s \frac{1}{N} \sum_{i=1}^{N} t_i - t_0 \tag{5.12}$$

Then a matrix S is formulated as (5.13), whose rows are the difference between the position of hydrophone i and the remaining three, and a Δ vector is expressed as (5.14), containing all combinations of TDOA between hydrophone i and the remaining.

$$S = \begin{bmatrix} r_i - r_j \\ \cdots \end{bmatrix} \tag{5.13}$$

$$\Delta = \begin{bmatrix} t_i - t_j \\ \cdots \end{bmatrix} \tag{5.14}$$

Taking into account the defined S and Δ, the signal's angle of arrival can be calculated from the direction of the signal, d, obtained from the least squares expression (5.15) [36]. Since there are only three equations to estimate three coordinates, then the expression is linear. It is important to notice that $(S^T S)$ has to be invertible, thus the rows which contain the chosen hydrophone configuration have to be linearly independent.

$$d = c_s \left(S^T S\right)^{-1} S^T \Delta \tag{5.15}$$

Having calculated the range ρ, given by the mean of the rr_i magnitudes in figure 5.1, and the direction d, the estimate of the transmitter position is given by the multiplication of these variables.

Finally, the plane wavefront estimator was integrated in a Monte Carlo method in order to execute multiple estimations of various transmitter positions, s, for a specific sensor configuration, so that it is possible to draw conclusions on its performance.

5.3 Fisher Information Matrix

The Fisher Information Matrix (FIM) serves to quantify the information that an observable variable is capable of returning to an estimator. This concept is intrinsically linked with the Crámer-Rao lower bound, which is a method that expresses the variance lower bound that a sensor configuration is capable of achieving, i.e. the best possible estimation precision it can achieve. Unlike the two previously presented processes, the Crámer-Rao bound is independent from the used estimator, as it assumes a linear estimator that is efficient and unbiased.

The fundamental process and mathematical notation previously used in 2.5.1 are applied in the procedure that will be explained next.

Firstly, the observation vectors are formulated based on an time of emission t_0, and the time of arrival based on the vectors that connect the hydrophone positions, r_i, to the transmitter, s. It is also considered an added noise component e_i, as defined in 3.2. The observations vectors are then expressed as (5.16).

$$t_i = t_0 + \frac{s - r_i}{c} + n_i \tag{5.16}$$

Then, all conditions are set to calculate the FIM, $I(d) \in \mathbb{R}^{3x3}$. In order to do so, if $\mathrm{d}_i = ||s - r_i||$ is the distance between each sensor and the source, the gradient of the observations vector can be expressed as shown in (5.17).

$$\nabla_d t(d) = \frac{1}{c} \begin{bmatrix} \frac{d_1^T}{||d_1||} \\ \frac{d_2^T}{||d_2||} \\ \vdots \\ \frac{d_N^T}{||d_N||} \end{bmatrix} \tag{5.17}$$

Additionally, the added noise component is present in the covariance matrix, represented as (5.18), which integrates the FIM equation.

$$\Sigma = \begin{bmatrix} \sigma_1^2 & 0 & 0 & 0 \\ 0 & \sigma_2^2 & 0 & 0 \\ 0 & 0 & \sigma_3^2 & 0 \\ 0 & 0 & 0 & \sigma_4^2 \end{bmatrix} \tag{5.18}$$

Overall, the conditions to obtain the FIM matrix are established and, after some algebraic manipulations, it can be expressed as (5.19). This function can be validated by a similar study made on TOA based optimal positioning [37].

$$I(d) = \frac{1}{c^2} \left[\sum_{n=1}^{N} \frac{d_i d_i^T}{||d_i||^2} \frac{1}{\sigma_i^2} \right] \tag{5.19}$$

The final step is to calculate the determinant and find its relation to the volume of the *uncertainty ellipsoid*. As mentioned in 2.5.1, the determinant of the FIM returns a deterministic value that represents the quantity of information that can be obtained for a certain position, therefore, the objective is to maximize $det(I(d))$.

The FIM can be associated with a physical meaning, more specifically an uncertainty volume that characterizes the variance that a specific configuration can achieve for an estimate. In an initial approach, the ellipsoid was not considered and instead it was approximated to an uncertainty sphere with the same volume. The radius of the uncertainty sphere, u_{sphere}, is expressed as (5.20). In this situation, the optimization objective is to minimize the uncertainty radius.

$$u_{sphere}(d) = \sqrt[2]{\sqrt[3]{det(I(d)^{-1})}} \tag{5.20}$$

In a further analysis, the uncertainty ellipsoid is calculated using (5.21). The squared eigenvalues of the inverse of the FIM indicate the length of each of the three ellipsoid axis and the eigenvectors specify the direction of each axis. An eigenvector that is associated with the smaller eigenvalue indicates the direction in which there is less uncertainty and, equivalently, an eigenvector whose eigenvalue is the larger represents the direction in which there is the biggest uncertainty. Consequently, the goal in this case is to minimize the uncertainty ellipsoid axis that corresponds to the maximum uncertainty.

$$u_{ellipsoid}(d) = \sqrt[2]{eig(I(d)^{-1})} \tag{5.21}$$

There are several optimality criteria that can be applied with the FIM in order to evaluate the estimation performance of a sensor configuration. Therefore, the selected metrics should be based on the intended application.

5.4 Performance Comparison between Methods

Upon presenting the theoretical details behind the three considered methods for evaluating configurations' performance, a further functional study will be presented through simulation results.

Throughout the functional demonstrations, three different hydrophone configurations are considered, A, B and C defined in 5.1, where the columns r_{Ai}, r_{Bi} and r_{Ci} contain the position's coordinates of each hydrophone i.

	r_{A1}	r_{A2}	r_{A3}	r_{A4}	r_{B1}	r_{B2}	r_{B3}	r_{B4}	r_{C1}	r_{C2}	r_{C3}	r_{C4}
x	0.02	0.02	0	0	0.1	0.1	0	0	0.1	0	0	0
y	0	0	0.1	-0.1	0	0	0.1	-0.1	0	0	-0.0707	0.0707
z	0.1	-0.1	0	0	0.1	-0.1	0	0	0	0.1	-0.0707	-0.0707

Table 5.1: Hydrophone configurations used for accuracy tests

In order to evaluate the performance of the configurations for the different methods, different criteria are considered, since the estimators and the FIM do not share the same evaluation metrics:

- **Evaluation criteria used for GBE and PWE**

  To illustrate a scenario where these estimators are applicable, we can consider that a vehicle is moving towards an acoustic signal transmitter whose position is unknown. Imagining that the target is at a minimum of few meters, then the main focus is to achieve an optimal bearing estimation which provides a more direct path and saves resources. The range estimation serves as secondary measurement that indicates how near the vehicle is from the destination, so that it is possible to make control decisions such as moderate the navigation speed in the proximity of the target. For the reasons outlined, the study that follows presents a more thorough analysis of the azimuth and elevation errors.

  For testing both estimators, a methodology was formulated in order to evaluate the accuracy that they achieve in defined circumstances. This approach is a Monte Carlo algorithm which allows to reiterate the estimation process according to the number of positions that are intended to be tested for a specific configuration, as well as create a series of repetitive calculations that allow to deduce the estimation error and turn the overall process more robust. The algorithm can be described as follows. For every defined position of the acoustic source, s, a function, that consists on the estimator, is called receiving as input the s, the positions of the hydrophone configuration, r_i, and an injected error e_i of $0.5\mu s$, that affects the ToA as detailed in 3.2. It then returns the estimated position of the source in Cartesian coordinates, $s_{cart}(x,y,z)$, and in spherical coordinates, $s_{sph}(n,\phi,\theta)$. As the position s in Cartesian corresponds to the real value that is intended to be estimated, we can also obtain the real spherical coordinates by directly converting s using the Cartesian to spherical relations in (5.22).

$$\begin{cases} n = \sqrt{x^2+y^2+z^2} \\ \phi = arctan\frac{y}{x} \\ \theta = arctan\frac{\sqrt{x^2+y^2}}{z} \end{cases} \tag{5.22}$$

Consequently all conditions are met to analyze the achieved error in each coordinate by comparing the real position to the estimated values as (5.23), where the observed coordinates are n, ϕ and θ.

$$error_{coordinate} = |estimated_{coordinate} - real_{coordinate}| \tag{5.23}$$

Additionally, the Mean-Squared Error (MSE) is also calculated in the spherical coordinates domain, which combines all errors in a single measurement.

- **Evaluation criteria used with the FIM**

  Several different optimality criteria can be applied using the FIM. Considering similar applications in literature [38], the evaluated criteria in the present work are the A-optimality, D-optimality and E-optimality, which are defined as follows:

  - **A-optimality**: minimizes the trace of the inverse of the FIM, therefore seeks the minimum average variance of the estimates.
  - **D-optimality**: minimizes the determinant of the inverse of the FIM, therefore the volume of the uncertainty ellipsoid. However, this can be misleading since the uncertainty in one direction can be much larger than the other directions, constituting a large FIM determinant which is not representative of the full estimation [28].
  - **E-optimality**: minimizes the largest eigenvalue of the inverted FIM, i.e. the ellipsoid axis with largest uncertainty. Since this criterion intends to minimize the axis that leads to the lower localization precision, then it is considered to be the most relevant in the present case (**RQ2**).

Upon defining the general simulation conditions, there are two types of simulations that will be performed :

- **Type SS (Specific Simulation)**, which is presented in this subsection, that compares the obtained performance result for each presented method when using a single configuration to estimate a specific transmitter position.
- **Type BS (Broad Simulation)** that tests the estimation of several positions with varying ranges, that form spheres around the origin of the coordinate axes, using multiple configurations for each of the methods.

5.4.1 SS Analysis

For the SS simulation, configuration C is used and the estimated position is $s_{cart}(100,0,0)$. Figures 5.3, 5.4 and 5.5 correspond to the estimate dispersion obtained for each of the previously presented methods. The green point in each plot represents the position that is being estimated. As indicated the first plot represents the side view, plane zx, and the third plot is the view from above, plane yx, which illustrate the norm error, the second plot represents the USBL front view, plane zy, which corresponds to the error in azimuth and elevation angle.

As can be observed, the estimate dispersion obtained with GBE demonstrates a larger deviation in norm estimation than the other methods, of about $4m$. Additionally, it is observed in the front view an azimuth deviation of approximately 2.3° and an elevation deviation of approximately 1.2°.

The PWE presents the estimate dispersion along a spherical surface, as expected since the method computes an average range. The norm estimation presents no significant deviation and the azimuth and elevation estimates show a similar dispersion as GBE.

The FIM plot presents the expected uncertainty axis obtained for the specific position estimation. From the three methods it presents the smallest uncertainty in all three coordinates, with a deviation of 0.21° in azimuth and 0.16° in elevation.

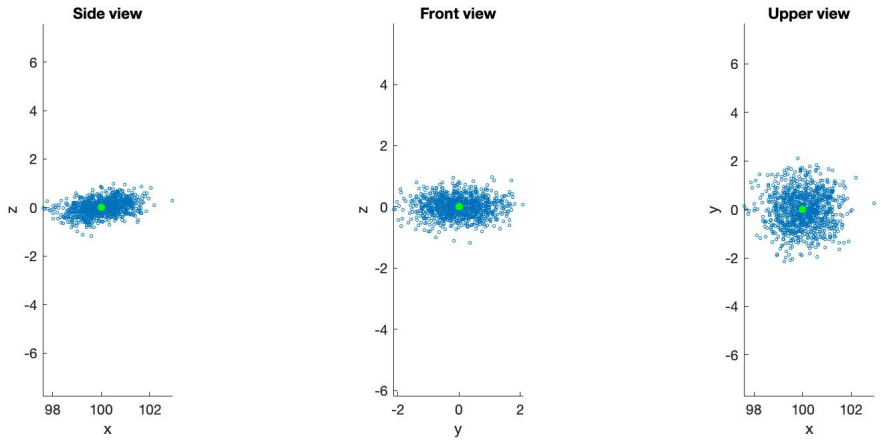

Figure 5.3: Estimate dispersion obtained with GBE for position $s_{cart}(100,0,0)$ using configuration C

Overall, for a position situated at a distance of $100m$ the PWE method achieves a estimate dispersion format similar to the FIM in terms of norm estimation and an approximately equivalent dispersion to the GBE in terms of azimuth and elevation deviation.

5.4.2 BS Analysis

In the BS, the considered positions for the acoustic source, s, are originally defined in spherical coordinates, s_{sph}. These positions are arranged so that for each defined norm, the elevation component covers the interval [-90° , 90°] in steps of one and, for each elevation value, the azimuth

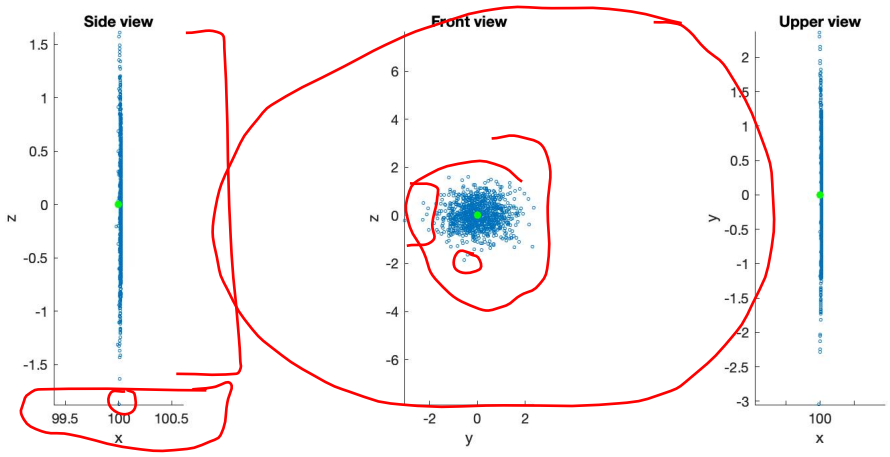

Figure 5.4: Estimate dispersion obtained with PWE for position $s_{cart}(100,0,0)$ using configuration C

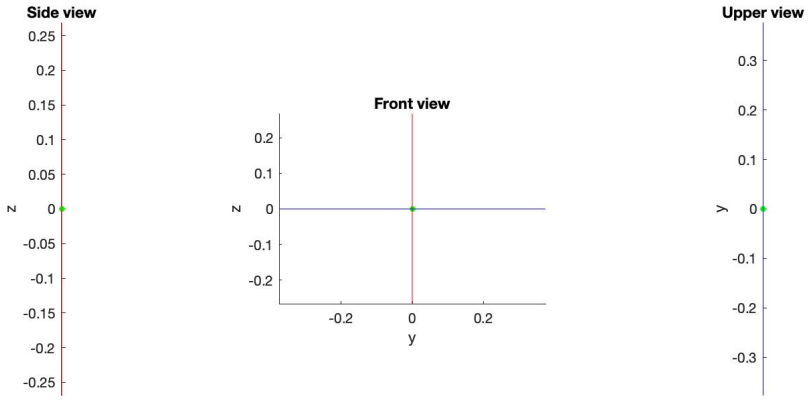

Figure 5.5: Estimate dispersion obtained with FIM for position $s_{cart}(100,0,0)$ using configuration C

component covers the interval [-180° , 180°] in steps of one, forming partial spheres around the reference axis' origin.

Then for each method, configurations A, B and C are tested for norms equal to $1m$ and $1000m$, that represent short and long range respectively. From each simulation using the estimators, the collected metrics are:

- **Mean squared error** (MSE): Incorporates both the variance and the bias of the estimator;
- **Standard deviation of the error** (σ): Indicates how disperse are the estimates from the expected value;
- **Maximum error**: Indicates the maximum error that is obtained by the estimator, thus the worst precision achieved.

Since the Crámer-Rao lower bound does not contemplate the azimuth and elevation errors as an optimality criteria, then other metrics are used in this case, which are the A-, D- and E-optimality, explained in 5.3. Therefore, from all the tested positions, the collected measurements correspond to the following parameters:

- **Max Determinant**: Denotes the maximum uncertainty volume achieved for a specific position;
- **Determinant Standard Deviation**: Indicates the standard deviation of the ellipsoid uncertainty volumes computed for all positions s;
- **Min Max Eigenvalue**: Indicates the smaller value from the larger uncertainty axis obtained for each position;
- **Min Trace**: Denotes the minimum sum of the uncertainty axes magnitudes

Tables 5.2, 5.3 and 5.4 summarize the collected data using the GBE, the PWE and the FIM, respectively.

			Azimuth		Elevation	
Configuration	Norm	MSE	Standard Dev	Maximum	Standard Dev	Maximum
A	1	0.767	0.841	10.102	0.259	1.954
	1000	0.759	0.751	9.243	0.255	1.879
B	1	0.197	0.183	2.206	0.059	0.376
	1000	0.199	0.186	2.186	0.061	0.368
C	1	0.201	0.184	2.277	0.061	0.412
	1000	0.232	0.215	2.334	0.071	0.438

Table 5.2: Obtained errors for configurations A,B and C by GBE

			Azimuth		Elevation	
Configuration	Norm	MSE	Standard Dev	Maximum	Standard Dev	Maximum
A	1	9.547	15.054	169.741	3.228	16.542
	1000	2.111	14.277	37.660	3.461	7.665
B	1	2.233	1.054	8.546	0.690	3.708
	1000	0.582	0.561	6.581	0.204	1.740
C	1	1.982	1.887	20.133	0.624	3.584
	1000	0.726	0.642	9.855	0.218	2.029

Table 5.3: Obtained errors for configurations A,B and C using PWE

		Determinant		Max Eigenvalue	Trace
Configuration	Norm	Max	Standard Dev	Min	Min
A	1	4.2×10^{-3}	6.65×10^{-4}	5.3×10^{-3}	5.60×10^{-5}
	1000	0.421	0.067	5.310	56.325
B	1	2.5×10^{-3}	8.78×10^{-5}	5.3×10^{-3}	5.17×10^{-5}
	1000	0.2462	0.008	5.306	56.283
C	1	3.0×10^{-3}	1.39×10^{-4}	7.1×10^{-3}	8.42×10^{-5}
	1000	0.290	0.014	7.410	84.882

Table 5.4: Obtained errors for configurations A,B and C by Crámer-Rao lower bound

By inspection, it is possible to observe that for both the GBE and PWE, the maximum deviations are considerably distant from the standard deviation, which correspond to positions in space with elevation values around -90° and 90° where it is achieved the worse estimation precision. Furthermore, while the minimum deviations in both estimators are similar, the PWE reveals much larger maximum errors since there are regions of space for which its localization accuracy is much lower.

Regarding the PWE, it should also be noted that the obtained standard deviations for short range of $1m$ are visibly higher than for long range of $1000m$, as expected since the approximation to the plane wavefront is only valid for long distances.

Finally, as the Crámer-Rao lower bound contemplates the best possible estimation precision for a sensor configuration, then the collected values for this case are consequently lower than the previous methods.

5.4.3 Further Behavioral Analysis

Having analyzed the performance of the studied methods, there are still two factors that can be explored in order to further understand its impact on the estimation accuracy. The first idea explores the impact of the the ToA measurement on the position estimation and the second studies the influence of an increasing baseline of the geometric configuration on the estimation accuracy.

5.4.3.1 Impact of ToA measurement on position estimation

As previously mentioned, the GBE uses the approximation which allows all hydrophones to use the a reference ToA added by a TDoA, representing the total time it takes for a signal to travel between the transmitter and each hydrophone. However, for long range positions the ToA is consequently much larger in relation to the time differences of arrival. So, the hypothesis is that for these cases the ToA is irrelevant for the calculations so it can be discarded. Therefore, for the angle of arrival estimation it is only necessary to use the TDoAs.

In order to simulate this, the reference time ToA is substituted by $\frac{10^4 m}{1500 m/s}$, which corresponds to a distance of $10km$. The results demonstrated no visible change in the error of the estimate. However, for distances bellow $100m$ the impact of this approximation is noticeable. Therefore, it is considered that the hypothesis is valid.

5.4.3.2 Influence of increasing the configuration baseline

In this research work, the configuration baseline corresponds to the geometric distance between hydrophones. Until this point, there are several obtained results which demonstrate the influence of the used baseline on the estimation performance. However, there are no conclusions about the optimal baseline length that should be used. The goal of this test is to delineate the influence of increasing the hydrophones' baseline in the obtained error.

In order to execute this test, the GBE is used with configuration C. To create an increasing baseline along the tests, in each iteration the x coordinate of r_{C1} increases $0.01m$ in a total of 200

times, which makes up a displacement range between 0.1 and 2m. Each position generates 100 accumulated samples that result in a single measurement per configuration.

Plot 5.6 represents the collected errors for each of the described configurations, whose baseline is progressively increasing in a constant pace. As illustrated, the obtained errors decrease visibly in the first 100 tests, corresponding to a r_{C1} position between 0.1 and 1m, becoming considerably constant for further distances.

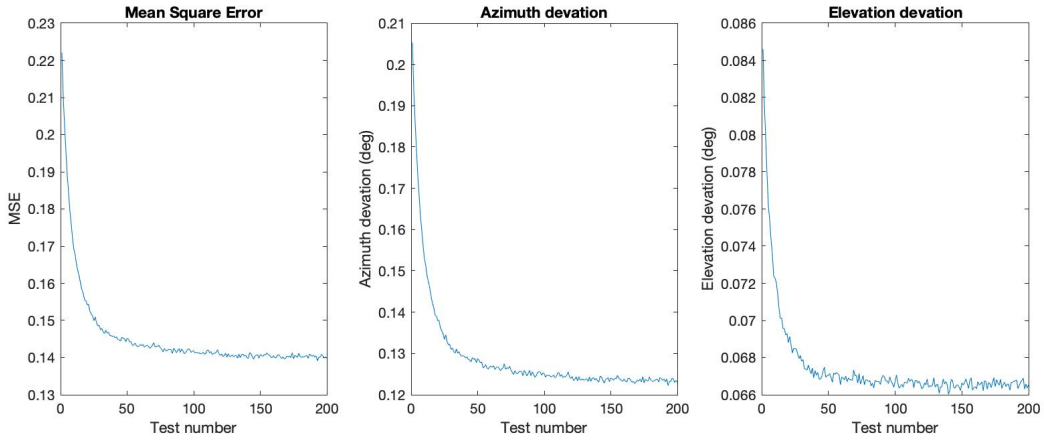

Figure 5.6: Error evolution with increasing baseline for r_{C1}

Additionally, the same experiment was done on hydrophone r_{C2} of the same structure, since its position on the configuration gets a different exposure than r_{C1} and a different outcome is expected. Having considered the same conditions as explained for the previous simulation, figure 5.7 illustrates the obtained results. It can be observed that the displacement of this specific hydrophone only causes an estimation improvement in the elevation deviation, it does not affect the estimation of the azimuth deviation and slightly increases the azimuth deviation. Therefore, an estimation improvement may not be achieved by distancing a random hydrophone, a study should be conducted for each particular configuration to determine which displacements lead to an enhancement.

In conclusion, it is proved that increasing the baseline of a configuration in specific cases may result in a decrement of the overall estimation error. However, this only occurs for a maximum distance after which the error variation is not significant .

5.4.3.3 Conclusions on behavioral analysis

The present chapter focused on a further analysis of the impact of some system characteristics to the estimation, involving mechanisms based on simulated results. Therefore, by way of summary, some main conclusions can be taken:

- As expected, the azimuth and elevation errors do not vary with the range of the transmitter's position, in contrast to errors in Cartesian coordinates which increase proportionally with the range;

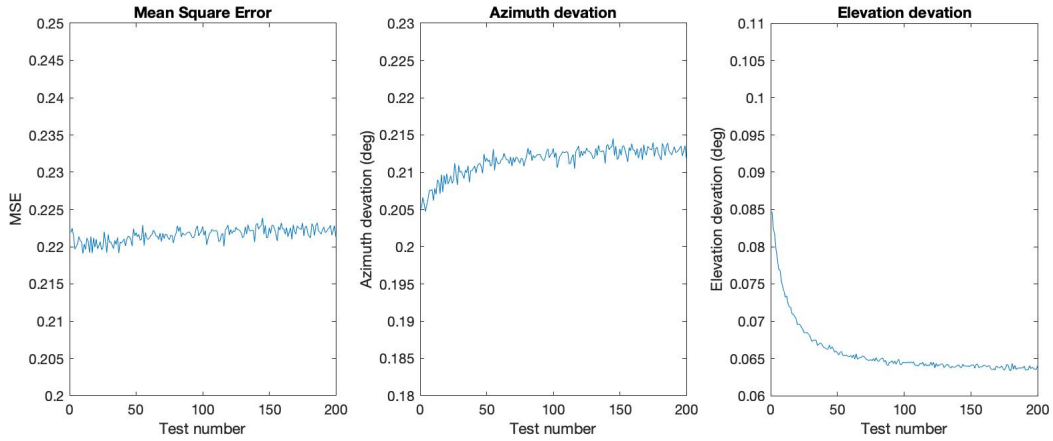

Figure 5.7: Error evolution with increasing baseline for r_{C2}

- The ToA measurement is not essential for long range distances. So, in those cases it can be discarded decreasing the dependency on the synchronization mechanism;
- Increasing the baseline of a hydrophone configuration can result in a better estimation, until reaching a certain distance after which the error becomes constant. Therefore, when choosing an hydrophone layout which can be limited to the dimensions of a physical structure, it does not have to be sought the maximum baseline possible but the length that leads to an error variation not significant ;
- The hydrophone configuration is a main factor on the estimation performance for any position in space. Although the characteristics that a configuration should meet to be optimal are still not clear, some aspects can be pointed out:
  - It is mandatory to ensure a sensor layout which covers three dimensions, so it is possible to estimate coordinates in 3D;
  - The positions of the sensors must not be coplanar to allow the application of the least squares method;
  - It is fundamental to have an adequate baseline which can be determined with the tool previously explained, to avoid singularities on the estimators and obtain lower estimation errors;
  - Bearing in mind that the configuration may be employed in real scenarios, it is useful to create schematics which require achievable distances between hydrophones and respect logical shapes to install in vehicles such as AUVs.

5.5 Final Remarks

This section focuses on three selected methodologies that are capable of evaluating sensor configurations' performance based on multiple criteria.

From the presented methods, it is expected that for short range estimation, distances from few centimeters to few meters, the GBE presents estimates that are more approximated to the real value than the PWE, since it uses the geometric relations between the hydrophone and the transmitter in order to estimate the position. Contrarily, for long range estimations, distances higher than a few meters, the PWE is expected to achieve lower estimation errors than the GBE, since it is a linear system and the approximation it considers does not affect the estimation.

Lastly, as the FIM reflects the quantity of information that a configuration is capable of acquiring in relation to a specific position, then it can be directly related to the accuracy of the estimation. The Crámer-Rao lower bound, which is intrinsically linked to the FIM, assumes the use of any unbiased and efficient estimator, which makes it a more generic tool. Consequently, it is widely used in literature for sensor configuration's performance analysis.

In conclusion, due to the generality of the tool, the FIM is considered the most efficient tool for this application (**RQ1**).

Chapter 6

Adaptive Configuration Selection Method

Having studied the estimator's behavior for several different configurations and conditions, there is still uncertainty about the best performance it can achieve. In the considered system, the hydrophone configuration has a decisive role on the achieved precision, as demonstrated. Therefore, a way to optimize the system's estimation would be to choose, for each position of the acoustic source, the configuration that returns the best estimation and thus the one that should be employed.

In a field scenario where a vehicle is searching for an acoustic transmitter, as it is navigating and readjusting its trajectory, the relative direction that is being estimated in real time is changing. Therefore, the system's performance can vary and arises the necessity of having a broader line of sight region from the hydrophones to the target. To resolve this issue, the proposed method assumes that the used USBL system integrates more than four hydrophones placed in known positions. This way, it is possible to reconfigure which four hydrophones are used at a time leading to an estimation that is the best possible for the available sensors (**RQ3**).

Another possibility is to determine through the same techniques which configuration of four hydrophones, tested in various positions along the vehicle, is the overall best for short and long range estimation. This can lead to a moderate compromise of the estimate accuracy, however decreases the number sensors that are employed and therefore the cost of the system.

This chapter is dedicated to explaining the methodological approach, the main findings and conclusions that were driven from the formulated optimal reconfiguration method. Firstly, the developed mechanism for defining line of sight regions for the deployed hydrophones is presented. Thereafter, the Monte Carlo method is explained, including the theoretical details as well as the developed algorithm. Then its functionality is demonstration through simulations that contemplate the three methods presented previously. Lastly, the implementation of the optimal solution based on range is presented and a practical comparison is established between the considered best configurations.

6.1 Line of Sight Definition

As briefly explained before, when considering a set of hydrophones placed in the surface of an AUV, there will be blind regions for each of the hydrophones. Nonetheless, when an acoustic source is positioned in a blind region of an hydrophone, it still can receive a transmitted signal through reflections on path objects or reverberation in the AUV's surface. Since these signals would be distorted from the original, they could lead to misinformation after the processing if they were to be considered. For this reason, it is essential to exclusively consider configurations whose hydrophones have line of sight (LOS) to the transmitter.

In the present application, this feature is executed through function $line\_of\_sight$ of algorithm 2, which outputs a vector containing all the hydrophones that have line of sight to the inputted transmitter position, $mean\_estimate$, from the considered set $matrix_{r_i}$.

In order to define which hydrophones have LOS to a specific position in space, a region was defined for each hydrophone as its LOS region, ls_i. Thus, three simplifications were initially considered:

- The model for the vehicle is an approximation to a typical shape of an AUV using geometric shapes, as represented in 6.1, composed by a cylinder as the body with $2 * w$ of diameter and a cone in the front with height equal to q;

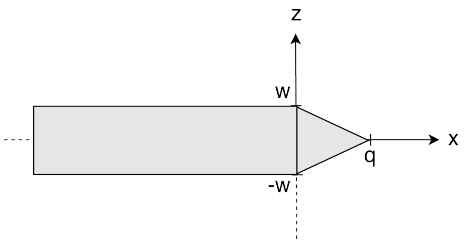

Figure 6.1: Model of AUV used to calculate the LOS region

- The regions for a $x \leq 0$ are defined as if the hydrophones were flat in the vehicle's surface, which leads to a simplified definition of the LOS region;

- Since hydrophone r_1 is integrated in every configuration, there is no necessity of defining its LOS region.

Having these relations into account, the LOS regions are then defined separately for $x \leq 0$ and $x > 0$. When $x \leq 0$, the second simplification previously mentioned is applied so all ls_i are defined as the region greater/less or equal than the tangential to the position of hydrophone i in plane yz. These tangential equations are defined in (6.1) to (6.8).

$$ls_2 \leftarrow x \leq 0 \ \wedge \ z > r_{2_z} \tag{6.1}$$
$$ls_3 \leftarrow x \leq 0 \ \wedge \ z < r_{3_z} \tag{6.2}$$
$$ls_4 \leftarrow x \leq 0 \ \wedge \ y > r_{4_y} \tag{6.3}$$
$$ls_5 \leftarrow x \leq 0 \ \wedge \ y < r_{5_y} \tag{6.4}$$
$$ls_6 \leftarrow x \leq 0 \ \wedge \ z \geq -y + w\sqrt{2} \tag{6.5}$$
$$ls_7 \leftarrow x \leq 0 \ \wedge \ z \leq y - w\sqrt{2} \tag{6.6}$$
$$ls_8 \leftarrow x \leq 0 \ \wedge \ z \geq y + w\sqrt{2} \tag{6.7}$$
$$ls_9 \leftarrow x \leq 0 \ \wedge \ z \leq -y - w\sqrt{2} \tag{6.8}$$

By evaluating these equations, it is possible to infer that the LOS regions for $x \leq 0$ intersect each other, as illustrated in figure 6.2. The projection is correspondent to the yz plane with an inverted y-axis, in accordance with the previously presented model of the USBL system. Additionally, each colored line corresponds to the LOS region covered by the hydrophone with the same color. For instance, if a transmitter is located in $s_{cart}(-10,-10,-10)$, by analysis of the schematic it is observable that this position is covered by ls_3, ls_5 and ls_9, thus in line of sight of hydrophones 3,5 and 9.

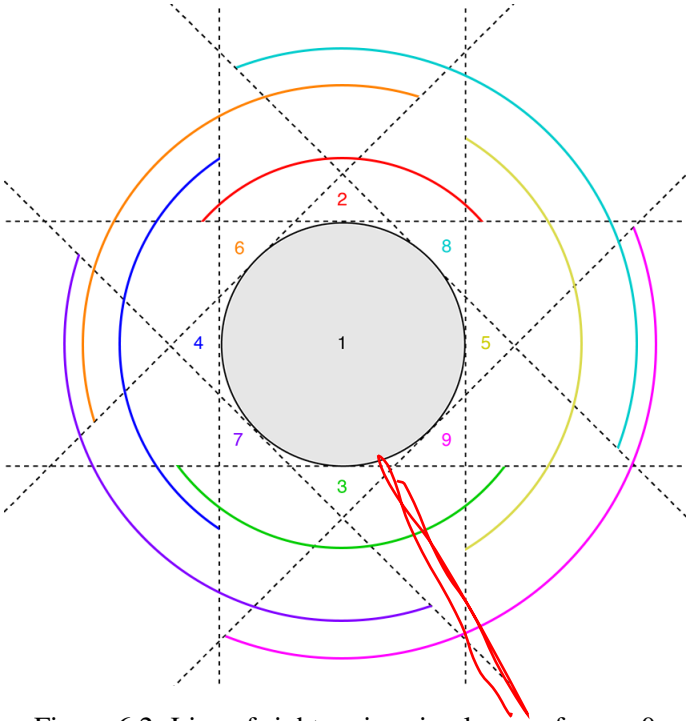

Figure 6.2: Line of sight regions in plane yz for x < 0

Analogously, when $x > 0$, all ls_i are defined as the region greater/less or equal than the tangential to the position of hydrophone i in planes xz or xy, depending on the hydrophone's location. Dealing with the hydrophones positioned in the y and z-axis, r_2, r_3, r_4 and r_5, it is

possible to directly formulate equations that help defining ls_2, ls_3, ls_4 and ls_5 since the tangent plane to these hydrophones is perpendicular to referential planes. However, when considering hydrophones r_6, r_7, r_8 and r_9, which are not positioned in any referential axis, the tangential plane which passes through the hydrophone and the front limit of the cone is not parallel to any of the referential planes xy, xz or yz. Therefore, the equations that could define these planes require a rotation of the referential axis. In order to counter this issue, since the shape of the model projected in the yz plane is a circle , if hydrophones r_6, r_7, r_8 and r_9 are rotated a 45° angle around the x-axis, they can become coincident with the positions of r_2, r_4, r_5 and r_3 respectively. Additionally, when considering this rotation, the position of the transmitter would also be rotated the same angle to maintain their relative positions. Overall, the used equations are defined by relations (6.9) to (6.12), where the regarded x, y, z coordinates are the original transmitter position for ls_2, ls_3, ls_4, ls_5, and the rotated transmitter position for ls_6, ls_7, ls_8, ls_9.

$$ls_2,\ ls_6 \leftarrow x > 0 \ \wedge \ z \geq -\frac{w}{q}x + w \tag{6.9}$$

$$ls_3,\ ls_9 \leftarrow x > 0 \ \wedge \ z \leq \frac{w}{q}x - w \tag{6.10}$$

$$ls_4,\ ls_7 \leftarrow x > 0 \ \wedge \ y \geq -\frac{w}{q}x + w \tag{6.11}$$

$$ls_5,\ ls_8 \leftarrow x > 0 \ \wedge \ y \leq \frac{w}{q}x - w \tag{6.12}$$

After evaluating these equations and the limiting planes that they form, the projected regions of LOS for r_2, r_3, r_4 and r_5 are illustrated in 6.3, where their intersection is evident. The regions ls_2, ls_3, ls_4 and ls_5 are naturally similar to these, with an additional rotation of 45° around the x-axis.

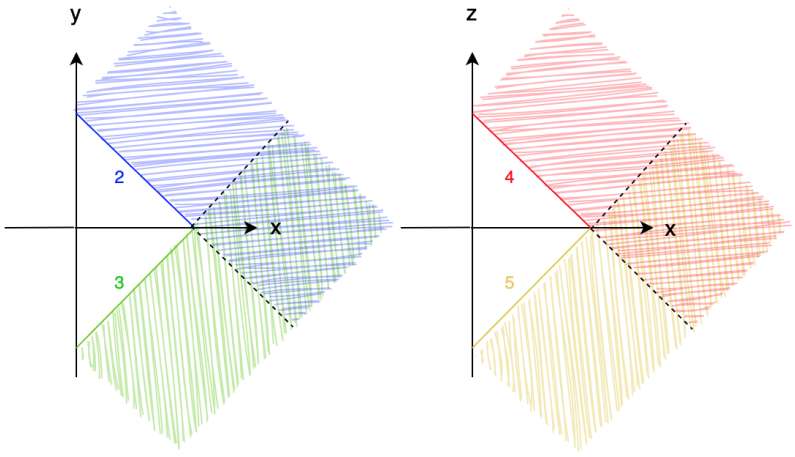

Figure 6.3: Line of sight regions in plane yx and zx for x $\geq$ 0

In summary, it is possible to deduce that there is a larger quantity of different configurations that cover the space for $x > 0$ than for $x \leq 0$ due to the model of the AUV and the considerations

described in the course of this subsection. Therefore it is expected a better estimation for positions of the acoustic source with an azimuth angle between $-90°$ and $90°$.

6.1.1 Practical Evaluation of the Line of Sight Regions

Upon inspecting the overall obtained results and the whole function of the system, a particular analysis is conducted on the mechanism that defines the hydrophones' LOS regions. As the estimation precision is not contemplated in this study, it is indifferent which estimation evaluation method is used for the simulations of this subsection. Therefore, all demonstrated results are performed with GBE.

The first position to be tested is $s(-10,-10,-10)$ which inherently has less hydrophones with line of sight, due to the method's limitation for $x \leq 0$. Additionally, since it is located in the seventh octant it is expected to be only in LOS with exactly three hydrophones, thus having only one available configuration with line of sight. After simulating, figure 6.4 is obtained which verifies the concepts described. The only configuration with line of sight is number 30, composed by r_1, r_3, r_5 and r_9.

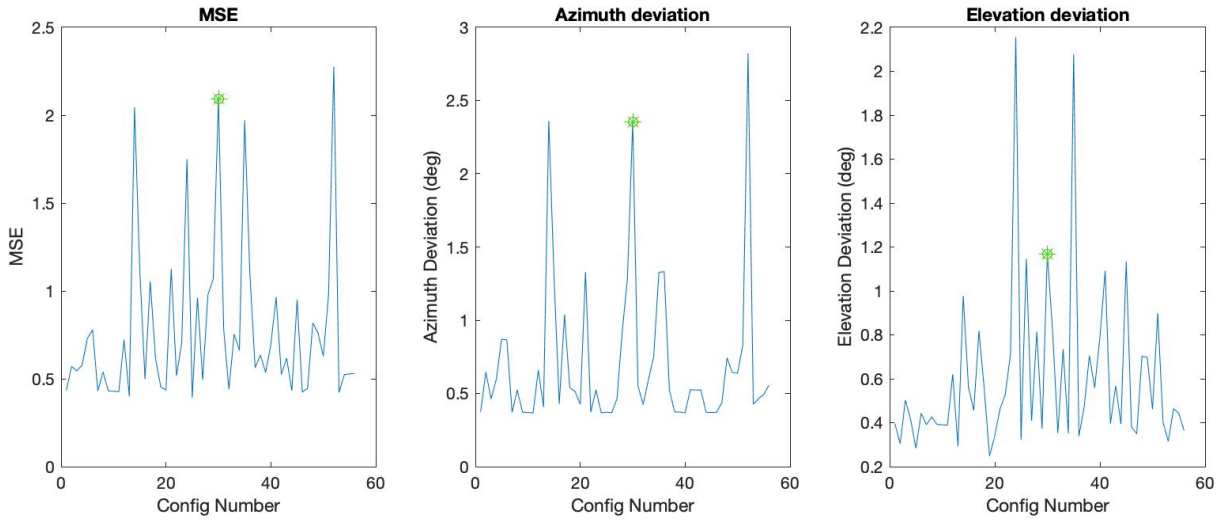

Figure 6.4: Errors obtained for all configurations when estimating position $s_{cart}(-10,-10,-10)$

Then, position $s(100,0,0)$ is tested. Due to its long range location and the fact that it is assumed a conic shape at the front of the vehicle, it is expected that this point has line of sight for every employed hydrophone. Figure 6.5 illustrates the simulated results which prove the theoretical expectation.

Lastly, an extensive verification process was held in order to ensure that the returned LOS hydrophones were plausible for many other positions. Table 6.1 summarizes this search, containing a total of eleven positions spread over each octant and the reference axis. By consulting the hydrophone map illustrated in 6.6, it is possible to confirm that for every selected position the returned hydrophones are the logically expected.

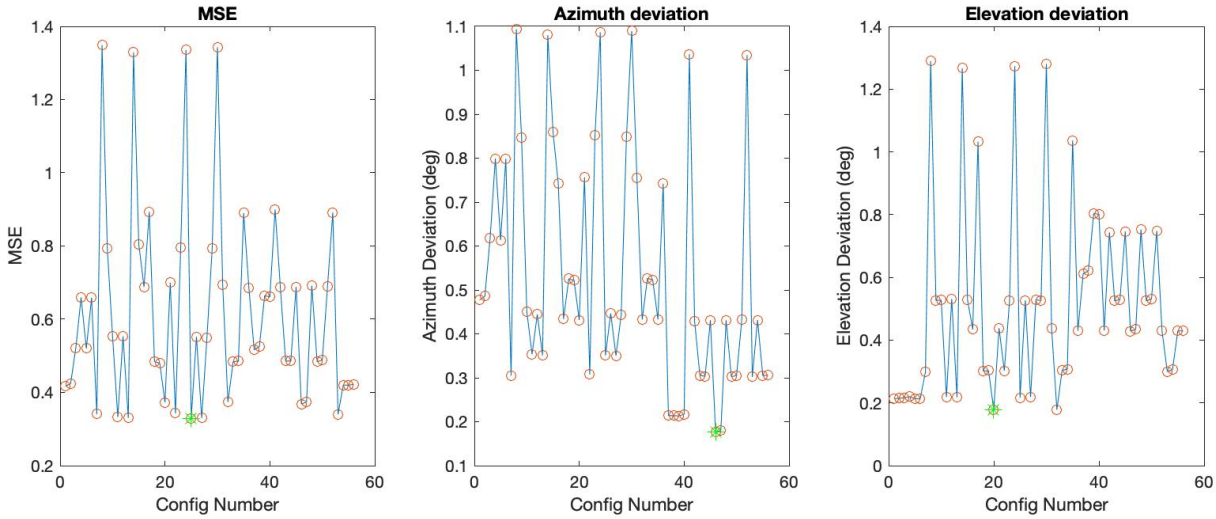

Figure 6.5: Errors obtained for all configurations when estimating position (100,0,0)

	s_x	s_y	s_z	Hydrophones with LOS
x-axis	100	0	0	2, 3, 4, 5, 6, 7, 8, 9
y-axis	0	100	0	4, 6, 7
z-axis	0	0	100	2, 6, 8
1^{st} octant	10	10	10	2, 4, 6, 7, 8
2^{nd} octant	5	5	-1	2, 3, 4, 6, 7
3^{rd} octant	1	-1	0	2, 3, 5, 8, 9
4^{th} octant	1	-10	-10	3, 5, 7, 8, 9
5^{th} octant	-100	10	10	2, 4, 6
6^{th} octant	-1	10	-5	3, 4, 6, 7
7^{th} octant	-1	-1	1	2, 5, 8
8^{th} octant	-1	-100	-10	3, 5, 8, 9

Table 6.1: Hydrophones with line of sight for several s positions

6.2 Monte Carlo Approach

The developed algorithm serves as a tool to determine which is the best available hydrophone configuration for a certain target position. This approach uses a Monte Carlo method which is useful to solve problems that are deterministic in nature through repetition and application of random parameters. Additionally, it makes use of the developed estimator, which is comprehensively explained in 5.1, to estimate the target position for each sensor configuration.

For this experiment, a total of nine hydrophones is considered, whose positions are contained in $matrix_{r_i}$, defined by table 6.2. Each column expresses the coordinates of each hydrophone, r_i, where the value of x_i is in the first row, the value of y_i in the second row and the value of z_i in the third row. Additionally, it is assumed $q = 0.1$, $w = 0.1$ and $e = \frac{\sqrt{2}}{2} * w$.

	r1	r2	r3	r4	r5	r6	r7	r8	r9
x	q	0	0	0	0	0	0	0	0
y	0	0	0	w	-w	e	e	-e	-e
z	0	w	-w	0	0	e	-e	e	-e

Table 6.2: Position coordinates for the implementation using 9 hydrophones

The presented hydrophone distribution was selected with no evidence of being superior to other possibilities and it tries to expand the traditional tetrahedral deployment, attending to the geometric characteristics of a torpedo-shaped AUV. The positions arrangement are represented in figure 6.6, where hydrophone r_1 is placed in front of the vehicle and hydrophones r_2 to r_9 form a circle with a w meters radius around the vehicle.

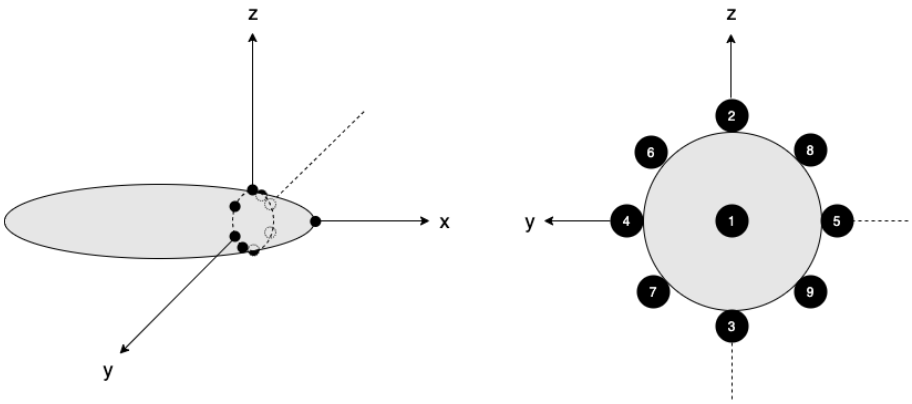

Figure 6.6: Hydrophone positions for the implementation using 9 hydrophones

Since the used configuration has to be non coplanar, it is defined that hydrophone r_1 integrates all the configurations, constituted by sets of four hydrophones, as it is the only one that covers a third dimension. Accordingly, the number of configuration possibilities is combinations of three out of eight, $C(8,3)$, making up a total of 56. Each of these configurations are associated with a

number from 1 to 56 and the hydrophones that integrate each of them are outlined in table A.1 for consultation when necessary.

Having the system presented, the algorithm will be explained next. For the sake of clarity, the algorithm was outlined in pseudo code and separated into two main parts, where 1 is integrated in 2.

Algorithm 1 Determines the average azimuth errors, elevation errors and MSE for a set of hydrophone configurations

1: **for** `all k configurations` **do**
2: **for** `all i estimation repetition` **do**
3: $estimator(s, config(k), error)$ {returns estimate in Cartesian and spherical coordinates}
4: `accum_estimate(i) ← result of the estimator in each repetition`
5: `accum_error_azimuth(i) ← azimuth error in each repetition`
6: `accum_error_elevation(i) ← elevation error in each repetition`
7: **end for**
8: $mean\_estimate \leftarrow \frac{accum\_estimate}{accum\_samples}$
9:
10: $deviation\_azimuth(config) = std(accum\_error\_azimuth)$;
11: $deviation\_elevation(config) = std(accum\_error\_elevation)$;
12: $error\_azimuth(config) = mean(accum\_error\_azimuth)$;
13: $error\_elevation(config) = mean(accum\_error\_elevation)$;
14:
15: $mse(config) = \sqrt{error\_azimuth(config)^2 + error\_elevation(config)^2}$;
16: **end for**

Algorithm 1 is dedicated to computing the average azimuth error, elevation error and MSE for each of the $k = 56$ hydrophone configuration, in order to understand which of them achieves the minimum deviations when estimating a specific position. In order to do so, for each possible hydrophone configuration, the chosen acoustic source position s was estimated $i = 1000$ times (line 3), using the developed estimator. This includes an injected error to the TDoA that follows a Gaussian distribution with zero mean and a configurable variance of σ^2, i.e., $e_i \sim \mathcal{N}(0, \sigma^2)$. The result of this repetition would be an estimate cloud around the absolute s position, which indicates the estimation variation achieved by a certain configuration for a specific position in space. At each stage of the repetition, the estimate is accumulated and the errors of azimuth and elevation are calculated, similarly to the process described in 5.4. Therefore, after computing all estimation repetitions, it is possible to extract four essential parameters that define the quality of the estimation for each configuration: a mean estimate (line 8); the azimuth and elevation standard deviations (lines 10 and 11); the azimuth and elevation estimation errors (lines 12 and 13); the MSE (line 15).

Finally, using the obtained parameters it is possible to determine three configurations that lead to the best estimation regarding MSE, azimuth deviation and elevation deviation. However, there are two main issues that this simple algorithm does not take into account:

1. For the considered system conditions, when testing the same position s multiple times, different hydrophone combinations are returned as the best option, which is an inconsistency

originated by introduced noise e_i.

2. Assuming that the hydrophone system is deployed in an AUV, it is expected that every hydrophone has a blind spot, where the acoustic source can be located. Even though the transmitted signals could still be received by these hydrophones, they would be distorted and could lead to misinformation so they should not be considered. Consequently the hydrophones that do not have line of sight to the transmitter should be disregarded as well.

In order to resolve both these problems, a second part of logic was developed, which is translated in pseudo code 2.

In order to turn this mechanism more robust and solve the first issue, it is considered that the experiment of algorithm 1 has to be reiterated a defined number of times to obtain coherent and conclusive answers. Having said this, algorithm 2 begins with a loop that reiterates $j = 10$ times the logic previously explained. Addressing the second issue, the *line_of_sight* function (line 7) is called, serving as filter to determine which hydrophones have line of sight to the estimated position. The mathematical definitions and conditions included in this function as well as the inputs and outputs are better clarified in the next subsection 6.1. Thereafter, all configurations that have full line of sight to the transmitter are extracted. Meanwhile, the azimuth deviations, elevation deviations and MSE are accumulated in each experiment reiteration (line 8 to 10) so that it is possible to obtain the definitive mean of these parameters for each configuration (line 12 to 14).

At this stage, it is possible to know already which are the configurations that are considered to achieve the minimum errors in each j reiteration and how many times each of them are chosen. However, these are still not filtered, thus they can contain occluded hydrophones, i.e. that do not have line of sight to the acoustic source. Consequently, the next step is to extract only the configuration with full LOS and form three matrices with the azimuth deviations, elevation deviations and MSE of these configurations. Having the final parameters calculated and filtered, the overall best configurations for each of the chosen parameters are given by the minimum of the matrices that contain said parameter (line 19 to 21), i.e. for all configurations with full LOS:

- The minimum obtained MSE corresponds to the configuration that more precisely estimates the position s in terms of MSE;
- The minimum obtained azimuth deviation corresponds to the configuration that more precisely estimates the position s in terms of azimuth;
- The minimum obtained elevation deviation corresponds to the configuration that more precisely estimates the position s in terms of elevation.

Additionally, it is possible to obtain the best configuration in terms of azimuth and elevation simultaneously, by computing the mean between the deviation of azimuth and elevation in each of the selected configurations. The minimum value obtained corresponds to the configuration which achieve the minimum the deviation in both parameters simultaneously.

Algorithm 2 Determines the overall best configuration for a specific position estimation considering:
- multiple full experiments (Algorithm 1);
- only hydrophones with line of sight to the target.

```
for all j experiment reiterations do
    *************************
    *** INSERT ALGORITHM 1 ***
    *************************

    line_of_sight(mean_estimate, matrix_ri) {returns which hydrophones have line of sight to the target}

    reit_mse = reit_mse + mse
    reit_dev_azimuth = reit_error_azimuth + deviation_azimuth
    reit_dev_elevation = reit_error_elevation + deviation_elevation
end for
mean_MSE = reit_mse ÷ j
mean_dev_azimuth = reit_dev_azimuth ÷ j
mean_dev_elevation = reit_dev_elevation ÷ j

Extract the configurations that contain only hydrophones with line of sight
Form matrix with errors of only the configurations with full line of slight

[best_config_for_mse, overall_min_mse] = min(overall_mse)
[best_config_for_azimuth, overall_min_dev_azimuth] = min(overall_dev_azimuth)
[best_config_for_elevation, overall_min_dev_elevation] = min(overall_dev_elevation)
```

6.3 Performance Comparison between Geometric Configurations

For the purpose of demonstrating the functionality of the developed adaptive configuration selection method, two types of simulations will be performed :

- **Type SS (Specific Simulation)** that generates the estimation of a specific transmitter position using several configurations and compares the obtained estimation precision and best configuration by each of the three methods presented in chapter 5.
- **Type BS (Broad Simulation)** that generates the estimation of several positions with short and long ranges, that form spheres around the origin of the coordinate axes, for an increased number of configurations. Then the obtained best configurations for specific defined criteria are compared for the three methods presented in chapter 5.

Similarity to 5.4, the evaluated criteria for the GBE and PWE are the achieved MSE, azimuth deviation and elevation deviation, whereas for the FIM the chosen optimality criteria is A-, D- and E-optimality.

6.3.1 SS Analysis

The simulations run in this subsection evaluate the estimation precision achieved by the 56 configurations defined previously, for the specific transmitter position $s_{cart}(10,10,10)$.

The plots that will be presented throughout the study show the metrics values for each configuration, highlighting the computed best configuration in each case. The plots can be interpreted as follows:

- The configurations marked with a red circle correspond to those whose hydrophones have line of sight to the transmitter;
- The green star indicates the configuration that achieves the lowest estimation error, i.e. the best configuration for the contemplated metric;
- When the azimuth and elevation deviations are evaluated simultaneously, the obtained plots are overlaid for a clear comparison between results, which can be interpreted as follows:
  - The azimuth deviation in degrees is represented by the blue line;
  - The elevation deviation in degrees is represented by the pink line;
  - The cyan diamond reveals which of the configurations leads to the minimum mean between the azimuth and the elevation deviations.

When running this experiment for the GBE, plot 6.7 is obtained.For the present case, the hydrophones considered to have line of sight to the target are r_2, r_4, r_6, r_7 and r_8. The configuration with lowest MSE and azimuth deviation is number 8, composed by hydrophones r_1, r_2, r_4 and r_6, which are the directly closer to the target. The configuration that originates lowest elevation deviation is number 19, composed by r_1, r_2, r_7 and r_8, which maximizes the baseline of the sensors with line of sight.

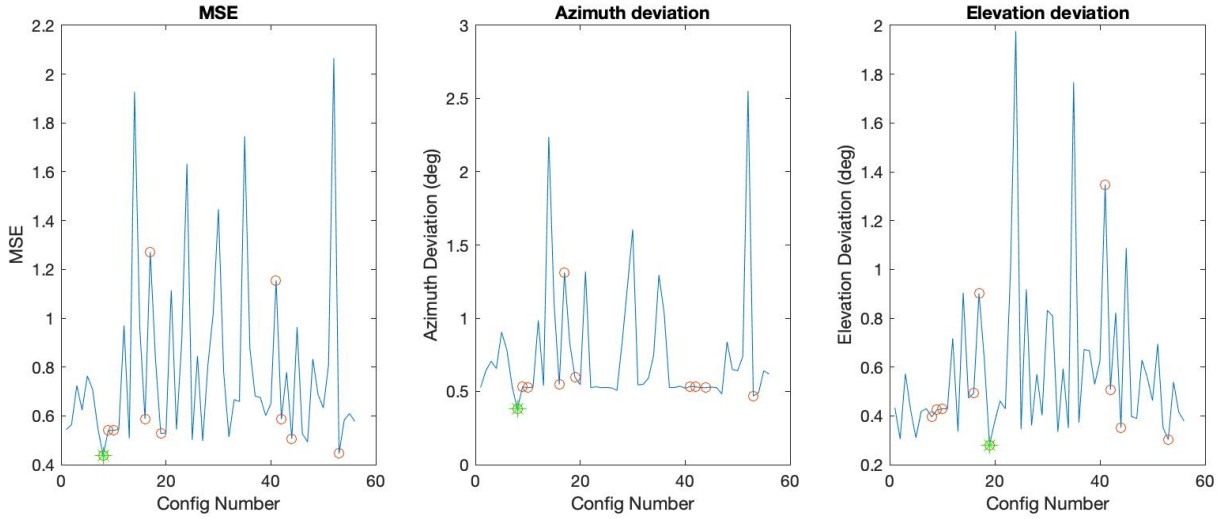

Figure 6.7: Errors obtained for all configurations when estimating position $s_{cart}(10, 10, 10)$ using the GBE

Additionally, figure 6.8 represents the overlaid azimuth and elevation deviations obtained with the GBE. In this case, the best configuration corresponds to number 53 which reaches a mean deviation of 0.385°.

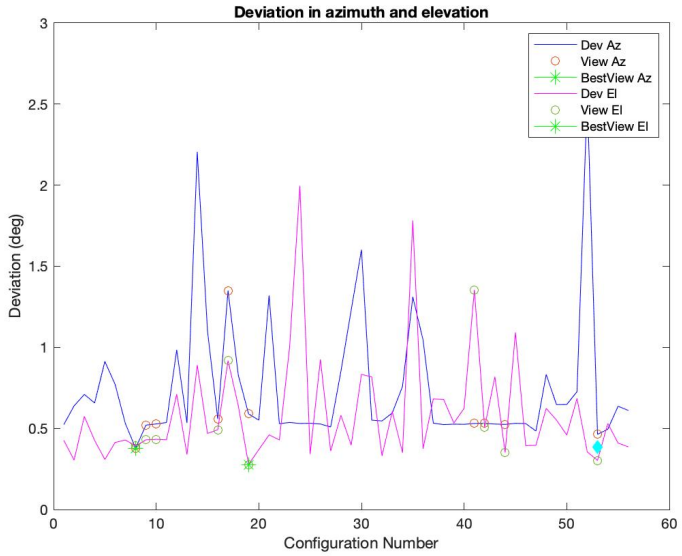

Figure 6.8: Overlaid azimuth and elevation deviations for all configurations when estimating position $s_{cart}(10, 10, 10)$ using the GBE

Alternatively, the same experiment was done using the PWE. The results of the simulation show that the same set of hydrophones have line of sight to the transmitter, as expected. Plot 6.9 corresponds to the obtained configurations' estimation precision. As can be observed the lowest MSE and azimuth deviation is number 53, which maximizes the baseline of the sensors with line of sight. The configuration that originates lowest elevation deviation is number 19, similarly to the observed result for the GBE.

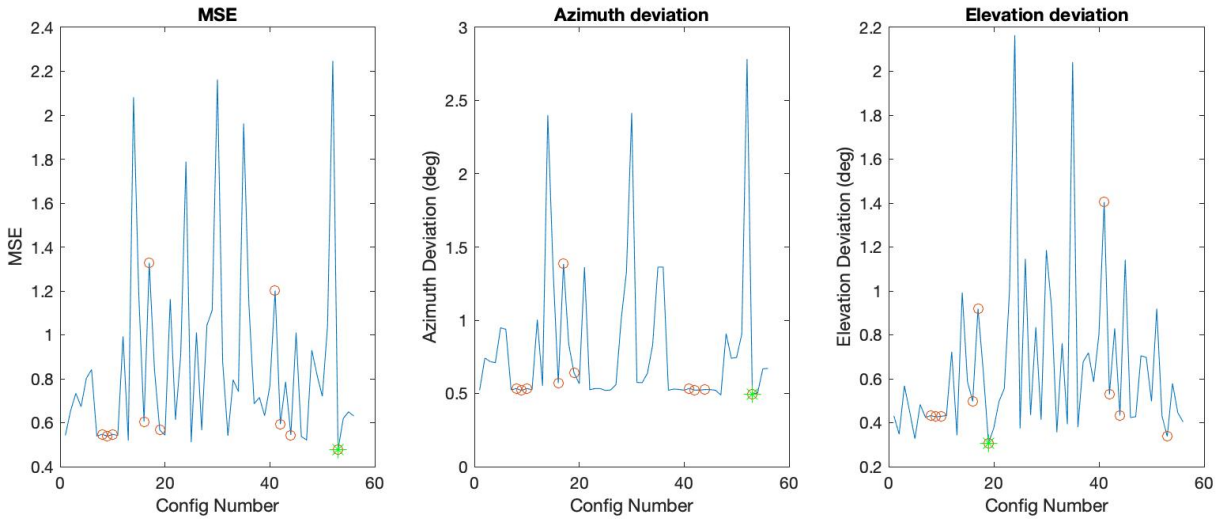

Figure 6.9: Overlaid azimuth and elevation deviations when estimating position $s_{cart}(10, 10, 10)$ using the PWE

Additionally, figure 6.10 represents the overlaid azimuth and elevation deviations obtained

with the PWE. In this case, the best configuration corresponds to number 53 which a mean deviation of 0.422°.

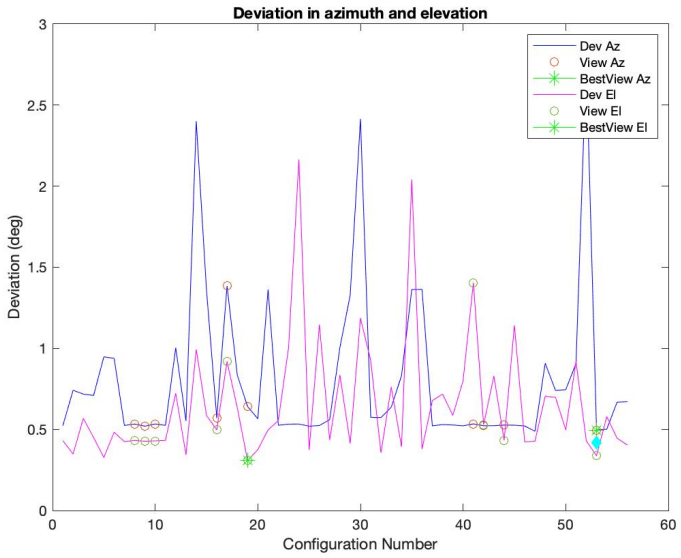

Figure 6.10: Overlaid azimuth and elevation deviations when estimating position $s_{cart}(10, 10, 10)$ using the PWE

Finally, the same experiment was performed using the Crámer-Rao lower bound with the A-optimality, D-optimality and E-optimality. The obtained results are illustrated in 6.11, which reveal matching best configurations with specific metrics for the GBE and the PWE. Accordingly, for the A- and D- optimality, configuration number 53 achieves the best estimation precision, with a summed uncertainty axis magnitude of $0.026m$ and uncertainty volume of 0.0164. For E-optimality, configuration number 8 is considered the most adequate achieving the minimum largest ellipsoid uncertainty axis among all configurations.

Upon investigating a specific position, several more individual positions were tested so that it would be possible to understand the behavior of the developed tool and generalize some of its characteristics. The main conclusions are summarized as follows:

- Configurations that achieve the overall minimum errors tend integrate the LOS hydrophones that attain among the larger distances between them, i.e. larger baseline;
- Transmitter positions that return a higher number of LOS hydrophones, have more possible configurations to choose from and therefore can be more optimized, presenting the lowest errors;
- The points directly behind the AUV, that cover positions with y and z in the range [-w,w], are not contained in any line of sight region. This results in a blind region for the formulated method, meaning that none of the hydrophones have line of sight to the transmitter. In such case, the signals may still be received with distortion, as mentioned in 6.1, decreasing the localization precision;

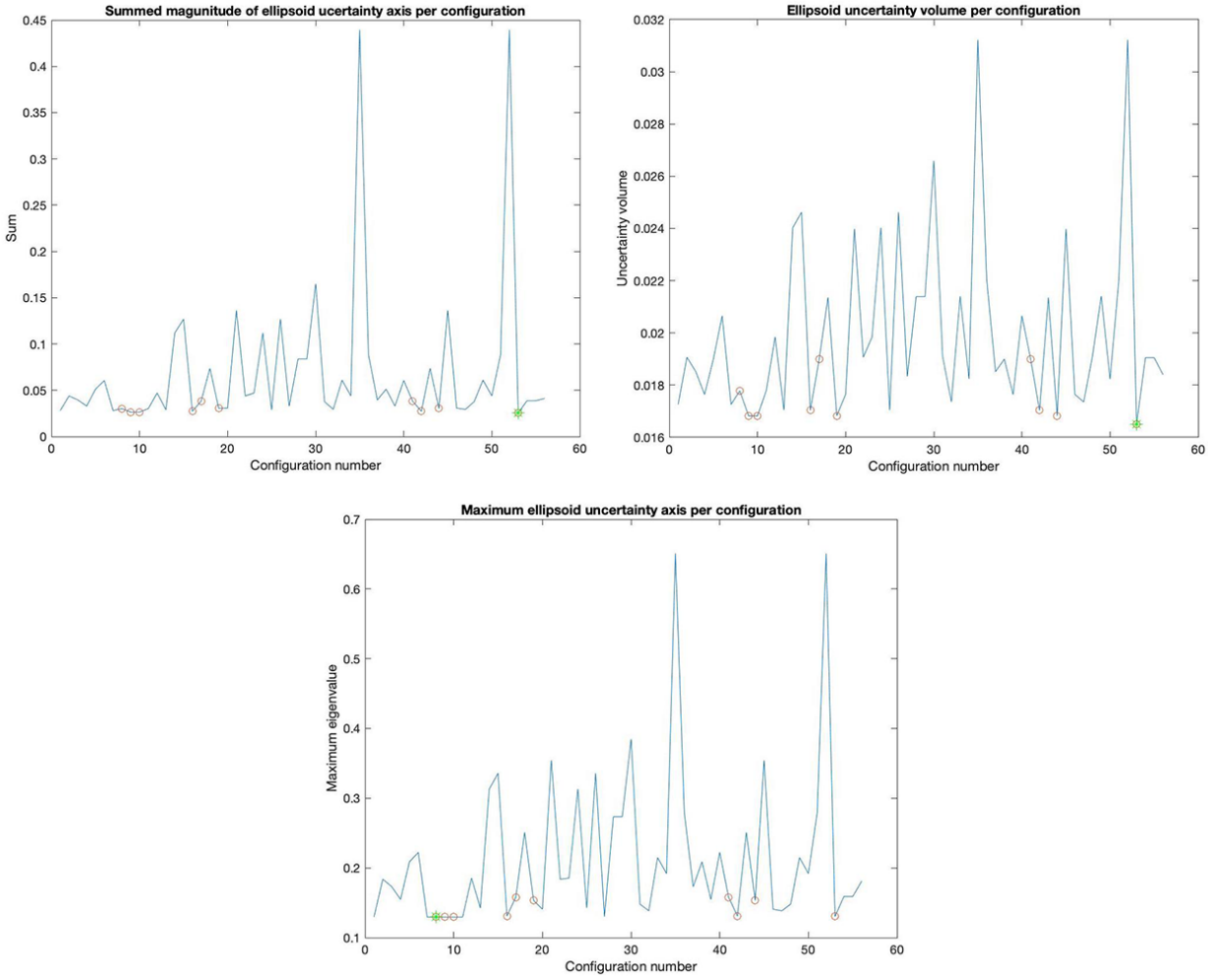

Figure 6.11: Overlaid azimuth and elevation deviations when estimating position $s_{cart}(10, 10, 10)$ using the FIM

- When the transmitter positions have $x \leq 0$, they are in line of sight of less hydrophones than for $x > 0$, so there are fewer possible configurations and the returned best option for the various parameters are more consistent. Consequently, the returned minimum errors are usually higher than for $x > 0$;
- Transmitter positions that are located near the y-axis, almost in parallel with the circle of hydrophones, are usually covered by only four LOS regions, which correspond to the sensors that are directly closer to the target.

6.3.2 BS Analysis

After analyzing the outcome of the estimations of a specific transmitter position, an alternate scenario can be explored. In the present work, an effort is made to improve the localization precision for both short and long range, so it is useful to evaluate the performance of several configurations not only for a single transmitter position but for the entire 3D space.

Therefore, this series of broad simulations intend to derive which configurations demonstrate the best performance when estimating a set of positions placed along a sphere with defined radius centered at the origin. This way, it would be possible to determine which configurations, from a discrete set, perform on average the best for short and long range.

In order to test this approach, some adjustments were considered from the conditions established in the system used thus far:

- It is assumed that the hydrophones are implemented in a structure that is invisible for the acoustic signals, thus all hydrophone positions have line of sight to any point in space;
- The number of possible hydrophone locations is increased for a more extensive study.

Once again, hydrophone r_1 is integrated in all configurations and a total of 24 possibilities are considered for the remnant three. These include the same 8 positions r_2 to r_9, established for the initial setup in table6.2, to which are added positions r_{10} to r_{25} defined in table 6.3. This addition corresponds to two replicated circles from the initial one, that assume the same y and z coordinates but are deviated from each other a dx equal to 20 centimeters. Figure 6.12 illustrates all the considered possible positions for the hydrophone's deployment. Accordingly, the number of possibilities is not correspondent to combinations of three out of 24, $C(24,3)$, since these contain non coplanar configurations. Therefore, the total number of available combinations to be tested is 1512.

The applied algorithm is similar to the previously explained algorithms 1 and 2, with the following variations:

1. An additional logical loop is added in algorithm 1 between lines 1 and 2, so that for each possible configuration all s are estimated a number of $i = 1000$ iterations.
2. the $line\_of\_sight$ function is no longer used, as it is considered that all hydrophones have line of sight to every position s.

	r_{10}	r_{11}	r_{12}	r_{13}	r_{14}	r_{15}	r_{16}	r_{17}	r_{18}	r_{19}	r_{20}	r_{21}	r_{22}	r_{23}	r_{24}	r_{25}
x	dx	dx	dx	dx	dx	dx	dx	dx	$2dx$	$2dx$	$2dx$	$2dx$	$2dx$	$2dx$	$2dx$	$2dx$
y	0	0	w	-w	e	e	-e	-e	0	0	w	-w	e	e	-e	-e
z	w	-w	0	0	e	-e	e	-e	w	-w	0	0	e	-e	e	-e

Table 6.3: Additional coordinates for an implementation with 25 hydrophones

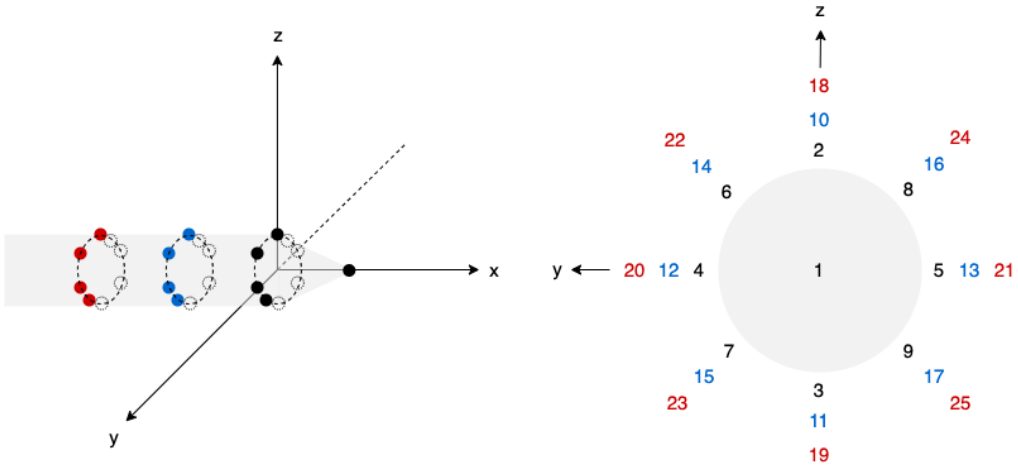

Figure 6.12: Hydrophone possible positions for optimality study based on range

The adapted algorithm was tested through a series of simulations, in which all 1512 defined configurations are used to estimate positions forming spheres of norms between $1m$ and $10000m$. In order to provide a more contextualized explanation of the subsequently simulation results, figure 6.13 is presented in advance, containing the most relevant representations that will be contemplated. This allows to visually associate the mentioned configuration numbers to the actual hydrophone placement throughout the following results description.

Firstly, simulations are performed for the GBE and the collected data is summarized in table 6.4.

The overall results do not exhibit a specific configuration to be the clear best in short or long range for the chosen parameters. For performance based on azimuth, configuration number 792 shows best results for norms between 1 and 10 meters. However, for longer range the results do not tend to a specific configuration, alternating between essentially three alternatives. Regarding performance based on elevation, only two configurations are specified in a very evident separation. Configuration 220 is indicated as the best for short range of 1 and 3 meters, while for longer ranges going from 10 to 10000 meters, configuration 260 is the clear nominated. As can be observed in the illustration, these are structurally similar. When evaluating azimuth and elevation accuracy simultaneously or MSE, the results are not clear and many configurations are alternated, where number 827 stands out as the most frequently indicated. In terms of error magnitude there is no

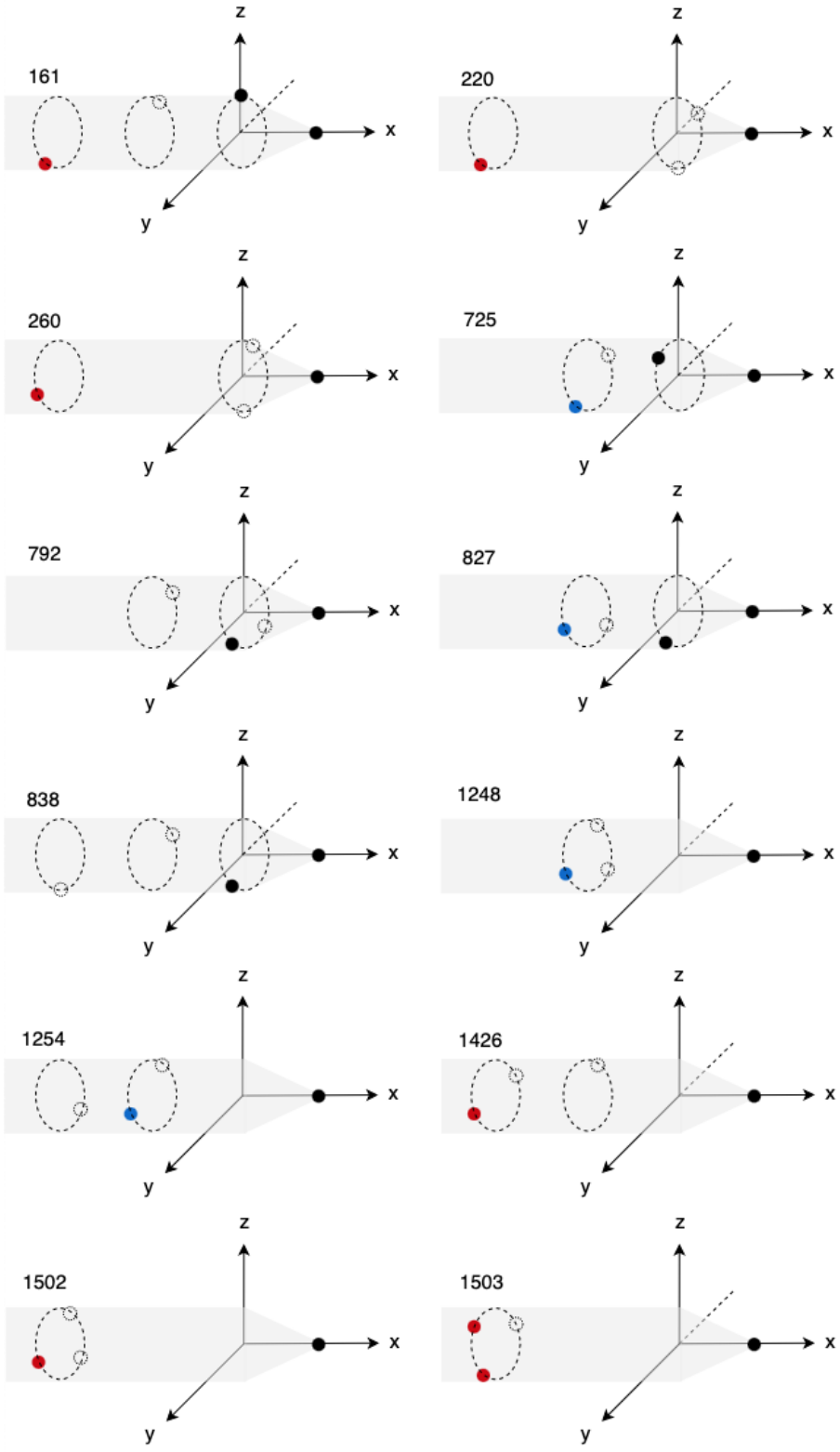

Figure 6.13: Illustration of relevant hydrophone configurations for range based estimation

	Azimuth		**Elevation**		**Azimuth+Elevation**		**MSE**	
Norm	Config	Min	Config	Min	Config	Min	Config	Min
1	792	0.4730	220	0.1758	862	0.3554	862	0.4654
2	792	0.4771	220	0.1738	827	0.3905	827	0.4549
3	792	0.4820	220	0.1752	827	0.3921	860	0.4571
10	792	0.4796	260	0.1702	827	0.3918	827	0.4572
20	827	0.4893	260	0.1702	827	0.3905	827	0.4537
50	792	0.4940	220	0.1705	860	0.3947	860	0.4615
100	860	0.4881	260	0.1707	827	0.3913	860	0.4538
200	827	0.4853	260	0.1706	827	0.3889	827	0.4511
500	792	0.4886	260	0.1722	929	0.3935	862	0.4606
1000	827	0.4846	260	0.1709	827	0.3899	827	0.4524
10000	792	0.4810	260	0.1724	862	0.3920	827	0.4554

Table 6.4: Results of Monte Carlo simulation for range based estimation using GBE

significant variation for an increasing norm.

Upon analyzing the GBE, a second experiment is run using the PWE. The collected data is summarized in table 6.5.

	Azimuth		**Elevation**		**Azimuth+Elevation**		**MSE**	
Norm	Config	Min	Config	Min	Config	Min	Config	Min
1	330	0.105	838	0.056	842	0.134	794	0.632
2	330	0.321	838	0.106	1206	0.390	794	0.668
3	330	0.528	838	0.150	725	0.397	531	0.644
10	1426	0.522	838	0.183	725	0.395	1015	0.580
20	725	0.537	1426	0.173	725	0.401	1254	0.539
50	1426	0.528	161	0.178	1254	0.402	1254	0.494
100	725	0.173	161	0.387	725	0.387	725	0.465
200	1426	0.519	161	0.176	725	0.397	725	0.483
500	1426	0.529	1426	0.182	725	0.393	725	0.474
1000	1426	0.502	161	0.181	1254	0.401	1254	0.483
10000	1426	0.544	1426	0.183	1254	0.398	1254	0.478

Table 6.5: Results of Monte Carlo simulation for range based estimation using PWE

For this case, there is also no clear best configurations for short and long range estimation regarding the chosen parameters. For the performance based on azimuth, configuration number 330 is indicated for short ranges between 1 and 3 meters, whereas for the remaining norms configuration number 1426 is the most frequently presented.For the performance based on elevation, configuration number 838 is indicated for short ranges between 1 and 10 meters, while for greater norms the layout alternated between numbers 1426 and 161. For remaining metrics, there is no unanimity or tendency in the indicated configurations, however numbers 725 and 1254 are the most frequent. In terms of error magnitude, the MSE presents a decreasing tendency with increasing norm, which is expected since for short range the approximation to a plane wavefront is not adequate. The remaining error magnitudes are approximated to the obtained data for GBE.

For the third experiment, the Crámer-Rao lower bound is used and the collected data is summarized in table 6.6. In order to clarify the notation, the stated parameters Eigenvalue, Determinant and Trace are correspondent respectively to the magnitude of the largest uncertainty axis, the uncertainty volume and the summed magnitudes of the uncertainty axis of the indicated configurations.

	E-optimality		**D-Optimality**		**A-Optimality**	
Norm	Config	Eigenvalue	Config	Determinant	Config	Trace
1	1248	6.2×10^{-3}	1503	1.6×10^{-3}	600	2.3×10^{-5}
2	1248	0.012	1503	2.5×10^{-3}	1426	9.2×10^{-5}
3	1248	0.018	1503	3.3×10^{-3}	1426	2.1×10^{-4}
10	1502	0.061	1503	7.4×10^{-3}	1426	2.4×10^{-3}
20	1502	0.121	1503	0.012	1426	9.6×10^{-3}
50	1502	0.303	1503	0.022	1426	0.061
100	1502	0.061	1503	0.034	1426	0.242
200	1502	1.212	1503	0.054	1426	0.968
500	1502	3.029	1503	0.100	1426	6.055
1000	1502	6.059	1503	0.159	1426	24.226
10000	1502	60.587	1503	0.737	1426	2.42×10^{3}

Table 6.6: Results of FIM simulation for range based estimation

By inspection, it is possible to observe that for each criterion there is a clear best configuration for short and long range contrarily to the most metrics of the previous results for GBE and PWE. Therefore, in terms of E-optimality configuration, an approximately constant error of 0.6% is visible, where number 1248 shows the best performance for short range between 1 and 3 meters, while for long range from 10 to 10000 meters configuration 1502 is indicated. For D-optimality, a single configuration, number 1503, was considered the best for all defined ranges,

which corresponds to an hydrophone placement that maximizes the baseline as illustrated in 6.13. Finally, in terms of A-optimality configuration number 600 is indicated for norm equal to 1 meters and, for the remaining ranges, number 1426 is chosen as the best option.

As mentioned before, the FIM method is considered the most reliable, as it does not depend on the selected estimator, and the results it presents demonstrate the most coherent configuration selection. It should be noticed that for all obtained results configuration number 1426 is coincident between the PWE and the FIM simulations, which leads to believe that it comprises favorable characteristics to an increased localization accuracy. However, as the E-optimality optimizes a more relevant optimization criteria, it is expected that configuration number 1502 demonstrates even better results.

6.4 Summary and Discussion

This chapter focuses on presenting the formulated adaptive configuration selection method, whose goal is to establish the sensor configuration that leads to the best estimation precision for a specific target position. After analyzing the results, it has proven to provide improved estimation accuracy by always selecting a configuration with line of sight to the target that achieves the lower estimation error.

An adaptation to this method is also explored in 6.3.2, whose goal is to select the sensor configuration that achieves the average best estimation for any target position along a sphere of defined norm. This allows to define optimal configurations based on the range, as demonstrated through simulations. As observed previously, the results of the Crámer-Rao lower bound demonstrate distinct optimal configurations for each optimality criteria in both short and long range.

This mechanism could be applied to a data muling scenario, as established in chapter 1. If a discrete set of hydrophones are deployed in an mule AUV, then it is possible to adapt the selected configuration depending on the perceived angle of arrival in real-time. This would allow to always use the configuration that leads to the lower estimation error and thus improve the localization accuracy.

Additionally, in a scenario where it is only relevant to have an average best estimation for both short and long range positions, then two configurations could be selected to be deployed. From the simulation results, considering the E-optimality as the most relevant criterion for this application, we can deduce that, for short range estimation, configuration number 1248 would be optimal, whereas, for long range, number 1502 would be preferred (**RQ4**).

Although configuration number 1502, illustrated in 6.13, does not present the absolute best performance for positions in the entire 3D space, it obtains sufficiently satisfactory results in general to be considered an adequate option for both short and long range estimation. Therefore, for this specific configuration using a norm of $1000m$, it is possible to estimate that using the GBE, the approximated maximum expected deviation for azimuth is 2°, elevation is 0.6° and norm is $6m$.

Chapter 7

Conclusions

This chapter is a reflection of all the work developed throughout this dissertation. All the conclusions are laid out and a brief overview of the develop work is described. Then the main contributions are presented followed by various aspects that could be further developed and explored in order to improve and continue the present research work.

7.1 Summary

As stated at the beginning, the overall aim of this research work was to develop a USBL system with characteristics that lead to an improvement on localization precision, both for short and long range.

Firstly, it is presented the implementation of an hardware module that computes with precision the time differences of arrival of acoustic signals received by a set of four hydrophones. The architecture demonstrated a significant decrease of the used resources comparatively to the previous implementation and a precise calculation of the time differences of arrival. After initial field tests, a rough estimation of the obtained precision leads to conclude that the ToA measurement was improved by using the phase differences along with the correlation.

Secondly, an adaptive configuration selection method was developed which is capable of determining the optimal configuration from a discrete set of fixed hydrophones, leading to higher localization precision, i.e. lower estimation error. It uses a Monte Carlo approach for a systematic comparison between a high number of configurations and to obtain averaged estimations for more coherent results. Additionally, as an effort to improve the USBL system's viewing angle, it was integrated a mechanism that assures the continuous selection of hydrophone sets that have line of sight to the transmitter positions. The simulated results show that the method as proven to be successful, since the selected configurations always correspond to the layout that leads to the lower estimation error.

Additionally, as initially intended, the method was adjusted so that it was possible to conduct a comprehensive study on the configurations that demonstrated to be optimal for short and long range. It was concluded that using the FIM together with the preferred optimality criterion for this

application, originated the most coherent results and allowed to elect the configurations that lead to an average higher precision.

This evaluation tool can be applied to any method that is capable of defining performance metrics for the evaluation of a sensor configuration. In the present research work three options were investigated, consisting on an estimator based on the TDoA measurement, an estimator that assumes a plane wavefront and the Crámer-Rao lower bound that uses the Fisher Information Matrix. From these three options, it was concluded that the most reliable would be the third due to the independence on the chosen estimator and its wide use on literature.

RQ1: *What method should be adopted in order to efficiently compare the performance of hydrophone configurations?*

In chapter 5, three different methods are contemplated as tools for evaluating hydrophone configurations performance. From the analysis, it is possible to understand that the GBE and PWE contain particularities that influence the results, namely the non-linearity and the assumed plane wavefront approximation, respectively. Alternatively, the FIM linearizes the estimation by considering any efficient and unbiased estimator, making it a more general tool that is widely employed for such application. For this reason, in the present research work the FIM is recognized as the most efficient and reliable tool for evaluating sensor configurations.

RQ2: *What decision metric(s) should be used to evaluate the optimal hydrophone configuration for a specific angle of arrival?*

Throughout the presented work, the used metrics for the simulations vary among the methods, including the azimuth error, elevation error and the mean-squared error for the estimators and the A-, D- and E-optimality for the Crámer-Rao lower bound, contemplated in 5.4. As the FIM is considered the most reliable tool to be used for configurations performance evaluation, then a closer look is taken into the optimality criteria in order to determine the most appropriate for localization estimation. As the A- and D-optimality can result in misleading conclusions, due to the disguise of data as previously explained in 5.4, then the E-optimality is ultimately considered to be the most relevant.

RQ3: *How should the system be developed in order to assure that the selected hydrophones always have line of sight to the transmitter?*

The proposed system assumes that the USBL system integrates multiple hydrophones deployed in known position along a vehicle, detailed in 6.2. Therefore, it is possible to reconfigure the set of four active hydrophones depending on the estimated angle of arrival, so that it is assured to always use hydrophones with line of sight to the transmitter, as described in 6.1. However, upon the formulation of the system, a blind region is identified directly behind the vehicle, which considering its dimensions, corresponds to a non significant percentage of the space.

RQ4: *Are there distinct best hydrophone configurations for short and long range estimation?* Upon the presentation of the developed method in 6.2, a dedicated set of simulations was performed in order to analyze the configurations performance based on the range of the acoustic transmitter instead of analyzing the angle of arrival of each individual considered position. Accordingly, recalling previous conclusions, the results obtained in 6.3.2 for the FIM using E-optimality reveal that configuration for short range configuration number 1248 achieves the higher estimation precision, whereas for long range, number 1502 is indicated as the best option from the considered possibilities.

Having all the proposed research questions answered, then the main hypothesis is recalled: *"Using a USBL system that reconfigures the hydrophone selection leads to an improvement on the underwater localization precision, allowing to always have a set of four active hydrophones with line of sight to the transmitter and makes it suitable for both short and long range estimation."*. From the presented results and main findings, it is possible to conclude that the developed mechanisms consist on an improvement on localization estimation precision, validating the proposed research hypothesis.

7.2 Contributions

The main contributions of this dissertation are:

- A digital signal processing module design with strict area constraints that receives signals from four different sensors and calculates the phase differences between them;
- A comparative study on three methods that evaluate the performance of sensor configurations based on several optimality criteria;
- The adaptive configuration selection method which is capable of determining the optimal sensor configuration, from a discrete set of hydrophones in fixed positions, that leads to highest localization precision, i.e. lowest estimation error.

7.3 Future Work

The developed work arose some innovative ideas and topics according to the state of the art on localization optimization methods.Consequently, there are several areas that can be further explored:

- Perform field experiments in order validate the developed adaptive configuration selection method;
- Implementing the developed algorithm for AoA estimation as a real-time system which can be used for real-time reconfiguration during underwater navigation;

- Using Machine Learning techniques in order to find the optimal hydrophone array configuration within a set spacial area, to be positioned in an underwater vehicle;
- Integrating the results in a Kalman Filter, which would mitigate singularities of the system.

Appendix A

Complementary Information

A.1 Hydrophone configurations numeration

In table A.1 it is possible to consult the composition of the configurations which are mentioned throughout the document. It includes the configuration number and the respective integrated hydrophones.

Table A.1: Configurations for the Monte Carlo approach with 9 employed hydrophones

Configuration number	Hydrophones
1	1 2 3 4
2	1 2 3 5
3	1 2 3 6
4	1 2 3 7
5	1 2 3 8
6	1 2 3 9
7	1 2 4 5
8	1 2 4 6
9	1 2 4 7
10	1 2 4 8
11	1 2 4 9
12	1 2 5 6
13	1 2 5 7
14	1 2 5 8
15	1 2 5 9

Table A.1

Configuration number	Hydrophones			
16	1	2	6	7
17	1	2	6	8
18	1	2	6	9
19	1	2	7	8
20	1	2	7	9
21	1	2	8	9
22	1	3	4	5
23	1	3	4	6
24	1	3	4	7
25	1	3	4	8
26	1	3	4	9
27	1	3	5	6
28	1	3	5	7
29	1	3	5	8
30	1	3	5	9
31	1	3	6	7
32	1	3	6	8
33	1	3	6	9
34	1	3	7	8
35	1	3	7	9
36	1	3	8	9
37	1	4	5	6
38	1	4	5	7
39	1	4	5	8
40	1	4	5	9
41	1	4	6	7
42	1	4	6	8
43	1	4	6	9

Table A.1

Configuration number	Hydrophones
44	1 4 7 8
45	1 4 7 9
46	1 4 8 9
47	1 5 6 7
48	1 5 6 8
49	1 5 6 9
50	1 5 7 8
51	1 5 7 9
52	1 5 8 9
53	1 6 7 8
54	1 6 7 9
55	1 6 8 9
56	1 7 8 9

References

[1] J. Liang, "Fifteen percent of ocean floor now mapped," Jun 2019. [Online] Available: https://www.deeperblue.com/fifteen-percent-of-ocean-floor-now-mapped/. [Accessed Oct. 28, 2019].

[2] H. P. Tan, R. Diamant, W. K. G. Seah, and M. Waldmeyer, "A Survey of Techniques and Challenges in Underwater Localization," *Ocean Engineering*, vol. 38, no. 1, pp. 1663–1676, 2011.

[3] F. B. Jensen, W. A. Kuperman, M. B. Porter, and H. Schmidt, "Fundamentals of Ocean Acoustics," in *Computational Ocean Acoustics*, pp. 3–17, Springer Science & Business Media, second ed., 2011.

[4] M. C. Domingo, "Overview of channel models for underwater wireless communication networks," *Physical Communication*, vol. 1, no. 3, pp. 163–182, 2008.

[5] M. Stojanovic and J. Preisig, "Underwater Acoustic Communication Channels: Propagation Models and Statistical Characterization," *IEEE Communications Magazine*, vol. 47, no. 1, pp. 84–89, 2009.

[6] J. M. F. M. aes, "Improving Time of Arrival Estimation Using Encoded Acoustic Signals," Master's thesis, Faculty of Engineering of the University of Porto, Porto, jul 2018.

[7] D. E. Chaitanya, C. V. Sridevi, and G. S. B. Rao, "Path loss analysis of Underwater communication systems," in *IEEE Technology Students' Symposium*, pp. 65–70, IEEE, 2011.

[8] S. Gezici, "A survey on wireless position estimation," *Wireless Personal Communications*, vol. 44, no. 3, p. 263–282, 2008. Springer Science & Business Media.

[9] C. Knapp and C. Glifford, "The generalized correlation method for estimation of time delay," *IEEE Transactions on Acoustics, Speech, and Signal Processing*, vol. 24, no. 4, pp. 320–327, 1976.

[10] B. M. R. Bharathi and A. R. Mohanty, "Underwater Sound Source Localization by EMD-Based Maximum Likelihood Method," *Acoustics Australia*, vol. 46, no. 2, pp. 193–203, 2018.

[11] A. Budiyono, L. Chen, S. Wang, K. McDonald-Maier, and H. Hu, "Towards autonomous localization and mapping of auvs: a survey," *International Journal of Intelligent Unmanned Systems*, 2013.

[12] V. Chandrasekhar, W. K. Seah, Y. S. Choo, and H. V. Ee, "Localization in underwater sensor networks - survey and challenges," in *WUWNet '06: Proceedings of the 1st ACM international workshop on Underwater networks*, pp. 33–40, 2006.

[13] V. Pierlot and M. V. Droogenbroeck, "A new three object triangulation algorithm for mobile robot positioning," *IEEE Transactions on Robotics*, vol. 30, no. 3, pp. 566–577, 2014.

[14] M. Erol-Kantarci, H. T. Mouftah, and S. Oktug, "A Survey of Architectures and Localization Techniques for Underwater Acoustic Sensor Networks," *IEEE Communications Surveys & Tutorials*, vol. 13, no. 3, pp. 487–502, 2011.

[15] X. You, Y. Wu, M. Zhu, X. Li, and L. Zhang, "Low Complexity Short Baseline Localization Algorithm Based on Taylor Expansion," in *2019 IEEE International Conference on Signal Processing, Communications and Computing*, pp. 1–5, IEEE, 2019.

[16] K. G. Kebkala and A. I. Mashoshinc., "AUV Acoustic Positioning Methods," *Gyroscopy and Navigation*, vol. 8, pp. 80–89, sep 2017.

[17] D. Sun, J. Ding, C. Zheng, and W. Huang, "An Underwater Acoustic Positioning Algorithm for Compact Arrays With Arbitrary Configuration," *IEEE Journal of Selected Topics in Signal Processing*, vol. 13, pp. 120–130, mar 2019.

[18] E. GmbH, "Underwater USBL Positioning Systems," 2018. [Online] Available: https://evologics.de/usbl. [Accessed Jan. 26, 2020].

[19] E. GmbH, "S2C Technology," 2018. [Online]. Available: https://evologics.de/s2c-technology [Accessed Jan. 26, 2020].

[20] E. GmbH, "18/34 communication and positioning devices," 2018. [Online]. Available: https://evologics.de/acoustic-modem/18-34 [Accessed Jan. 26, 2020].

[21] E. GmbH, "S2C R 12/24 USBL communication and positioning device," 2018. [Online]. Available: https://evologics.de/acoustic-modem/12-24/usbl-serie [Accessed Jan. 26, 2020].

[22] Sonardyne, "Micro-Ranger 2 Shallow Water USBL System," 2020. [Online]. Available: https://www.sonardyne.com/product/micro-ranger-2-shallow-water-usbl-system/ [Accessed Feb. 3, 2020].

[23] Sonardyne, "Mini-Ranger 2 Shallow Water USBL System," 2020. [Online]. Available: https://www.sonardyne.com/product/underwater-positioning-mini-ranger-2/ [Accessed Feb. 3, 2020].

[24] A. Acoustics, "Easytrak Alpha USBL System, Model 2665," 2020. [Online]. Available: https://appliedacoustics.com/wp-content/uploads/2019/10/Easytrak-Alpha-2665-Technical-Specification.pdf/ [Accessed May 3, 2020].

[25] K. Maritime, "HiPAP - High Precision Acoustic Positioning," 2016. [Online]. Available: https://www.kongsberg.com/maritime/products/Acoustics-Positioning-and-Communication/acoustic-positioning-systems/hipap-models/ [Accessed May 2, 2020].

[26] A. N. Bishop, B. Fidan, B. D. O. Anderson, K. Doğançay, and P. N. Pathirana, "Optimality analysis of sensor-target localization geometries," *Automatica*, vol. 46, no. 3, pp. 479–492, 2010.

[27] E. Rady, M. M. E. A. El-Monsef, and M. M. Seyam, "Relationships among several optimality criteria," *Interstat*, vol. 15, no. 6, pp. 1–11, 2009.

[28] S. Xu and K. Doğançay, "Optimal sensor placement for 3-d angle-of-arrival target localization," *IEEE Transactions on Aerospace and Electronic Systems*, vol. 53, no. 3, pp. 1196–1211, 2017.

[29] D. Moreno-Salinas, A. Pascoal, and J. Aranda, "Optimal sensor placement for acoustic underwater target positioning with range-only measurements," *IEEE Journal of Oceanic Engineering*, vol. 41, no. 3, pp. 620–643, 2016.

[30] Y. Zhang, S. Wang, and G. Ji, "A comprehensive survey on particle swarm optimization algorithm and its applications," *Mathematical Problems in Engineering*, vol. 2015, 2015.

[31] C. Tholen, T. A. El-Mihoub, L. Nolle, O. Ralle, and R. Rofallski, "Optimal receiver configuration of short-baseline localisation systems using particle swarm optimisation.," in *ECMS*, pp. 25–31, 2020.

[32] A. M. Bonito, "Acoustic System for Ground Truth Underwater Positioning in DEEC's Test Tank," Master's thesis, Faculty of Engineering of the University of Porto, Porto, jul 2019.

[33] J. Valls, T. Sansaloni, A. Perez-Pascual, V. Torres, and V. Almenar, "The use of cordic in software defined radios: A tutorial," *IEEE Communications Magazine*, vol. 44, no. 9, pp. 46–50, 2006.

[34] A. D. Poularikas, *Handbook of Formulas and Tables for Signal Processing*, ch. The Hilbert Transform. CRC Press, 1999.

[35] A. A. Assef, B. M. Ferreira, J. M. Maia, and E. T. Costa, "Modeling and fpga-based implementation of an efficient and simple envelope detector using a hilbert transform fir filter for ultrasound imaging applications," *Research on Biomedical Engineering*, vol. 34, no. 1, pp. 87–92, 2018.

[36] J. Reis, M. Morgado, P. Batista, P. Oliveira, and C. Silvestre, "Design and experimental validation of a usbl underwater acoustic positioning system," *Sensors*, vol. 16, no. 9, p. 1491, 2016.

[37] B. Ferreira, A. Matos, and N. Cruz, "Optimal Positioning of Autonomous Marine Vehicles for Underwater Acoustic Source Localization using TOA Measurements," in *2013 IEEE International Underwater Technology Symposium (UT)*, pp. 1–7, IEEE, 2013.

[38] Y. Zhang, Y. Li, Y. Zhang, and T. Jiang, "Underwater anchor-auv localization geometries with an isogradient sound speed profile: A crlb-based optimality analysis," *IEEE Transactions on Wireless Communications*, vol. 17, no. 12, pp. 8228–8238, 2018.